

# Automatic Mapping of Discontinuity Persistence on Rock Masses Using 3D Point Clouds

Adrián Riquelme<sup>1</sup>  · Roberto Tomás<sup>1</sup> · Miguel Cano<sup>1</sup> · José Luis Pastor<sup>1</sup> · Antonio Abellán<sup>2</sup>

Received: 24 January 2018 / Accepted: 19 May 2018 / Published online: 24 May 2018  
© Springer-Verlag GmbH Austria, part of Springer Nature 2018

## Abstract

Finding new ways to quantify discontinuity persistence values in rock masses in an automatic or semi-automatic manner is a considerable challenge, as an alternative to the use of traditional methods based on measuring patches or traces with tapes. Remote sensing techniques potentially provide new ways of analysing visible data from the rock mass. This work presents a methodology for the automatic mapping of discontinuity persistence on rock masses, using 3D point clouds. The method proposed herein starts by clustering points that belong to patches of a given discontinuity. Coplanar clusters are then merged into a single group of points. Persistence is measured in the directions of the dip and strike for each coplanar set of points, resulting in the extraction of the length of the maximum chord and the area of the convex hull. The proposed approach is implemented in a graphic interface with open source software. Three case studies are utilized to illustrate the methodology: (1) small-scale laboratory setup consisting of a regular distribution of cubes with similar dimensions, (2) more complex geometry consisting of a real rock mass surface in an excavated cavern and (3) slope with persistent sub-vertical discontinuities. Results presented good agreement with field measurements, validating the methodology. Complexities and difficulties related to the method (e.g., natural discontinuity waviness) are reported and discussed. An assessment on the applicability of the method to the 3D point cloud is also presented. Utilization of remote sensing data for a more objective characterization of the persistence of planar discontinuities affecting rock masses is highlighted herein.

**Keywords** Persistence · Rock mass · Characterization · 3D point clouds · Photogrammetry · LiDAR · Automatic extraction

## Abbreviations

DBSCAN	Density based scan
DS	Discontinuity set
DSE	Discontinuity set extractor
EIFOV	Effective instantaneous field of view
GPR	Ground penetrating radar
HDS	High definition surveying
ISRM	International Society for Rock Mechanics and Rock Engineering
JCS	Joint (wall) compressive strength
JRC	Joint (wall) Roughness coefficient
KDE	Kernel density estimation
LiDAR	Light detection and ranging
RMSE	Root-mean-square error

SfM Structure from Motion

TLS Terrestrial laser scanner

## List of symbols

$a_i$	Area of the $i$ th discontinuity in a 3D region of volume $V$
$a_{Ri}$	Area of the discontinuity $i$ within region $R$
$A$	First parameter of the general form of the equation of a plane
$A_R$	Total area of the region
$B$	Second parameter of the general form of the equation of a plane
$C_h$	Convex hull
$Cl$	Cluster
$D$	Fourth parameter of the general form of the equation of a plane
$I$	Intensity of discontinuities within a rock mass
$J$	Discontinuity
$k$	Numerical parameter that controls the sensitivity of the merging process of coplanar clusters
$K$	Discontinuity persistence

✉ Adrián Riquelme  
ariquelme@ua.es

<sup>1</sup> Department of Civil Engineering, University of Alicante, Alicante, Spain

<sup>2</sup> Institute of Applied Geosciences, School of Earth and Environment, University of Leeds, Leeds, UK

<i>m</i>	Mean
<i>n</i>	Number of data
<i>O</i>	Origin of a Cartesian coordinate system
<i>P</i>	Point
<i>R</i>	Region of a plane
<i>s</i>	Normal spacing
<i>V</i>	Volume of a region
<i>x</i>	First coordinate of a point in a Cartesian coordinate system
<i>X</i>	Set of points
<i>y</i>	Second coordinate of a point in a Cartesian coordinate system
<i>z</i>	Third coordinate of a point in a Cartesian coordinate system

#### Greek letters

$\alpha$	Dip direction angle of a discontinuity set
$\beta$	Dip angle of a discontinuity set
$\lambda$	Mean trace termination or persistence frequency
$\mu$	Mean of point-plane distances
$\sigma$	Standard deviation of the distances point-plane distances

## 1 Introduction

### 1.1 General Overview

Discontinuity is a general term in rock mass engineering, and denotes any separation in a rock mass characterized by low or non-existent tensile strength (Zhang 2006). These features are usually organized in pseudo-parallel surfaces referred to as joint sets or discontinuity sets (International Society for Rock Mechanics 1978), although the International Society for Rock Mechanics (ISRM) suggested the general term discontinuities instead of joints. The ‘Suggested Methods for the Quantitative Description of Discontinuities’ (International Society for Rock Mechanics 1978) of the ISRM defined the different types of discontinuities and suggested characterization methods, summarized in Table 1. Although these parameters are widely accepted by the scientific and technical community, advances in new technologies and new methodologies are changing how rock mass discontinuities are being investigated, as shown in Table 1.

Discontinuity persistence has a significant effect on rock mass strength, but is a difficult parameter to measure (Einstein et al. 1983). Traditional methods to measure discontinuity persistence were designed several decades ago, according to the existing available techniques and instruments (International Society for Rock Mechanics 1978) and are still widely applied *in situ* by engineers. The limitations of these methods are widely known, including the risks of

working on difficult and unstable platforms, the absence of access to outcrops and the subjectivity associated with direct measures (Slob et al. 2010). However, the recent acceptance of 3D remote sensing techniques such as light detection and ranging (LiDAR) instruments, digital photogrammetry or structure from motion (SfM) (Ullman 1979) is changing how rock slopes are being investigated. Digital photogrammetry is a well-known technique that enables the 3D study of the morphology of natural and engineered rock slopes (Sturzenegger and Stead 2009a). SfM is becoming an extremely important topic in the scientific community due to the availability of photogrammetrically derived point clouds in terms of the cost–benefit ratio of the equipment, ease of use and quality of results (Micheletti et al. 2015; Abellán et al. 2016).

3D point clouds captured from remote sensing techniques usually comprise millions of points that are defined by means of: (1) coordinates of each point of the surface on a local reference system; (2) intensity reflected by the surface and recorded by the sensor; and (3) possibility of automatic superposition of photographs captured during the scanning process, assigning an estimated colour (R, G, B) to each point. These digital datasets captured in the study area enable the analysis of rock mass features with the use of geometrical or radiometric parameters (e.g., intensity, visible colours, or other hyperspectral data) of rock masses. These data provide geometrical information (among other data) on the slope (e.g., natural, blasted or excavated) along with the visible discontinuities in the rock mass.

Although discontinuities are not planes but surfaces that present roughness and waviness (and could even present curved or undulatory shapes) (Dershowitz 1985), they are usually treated as planes when an appropriate study scale is used (International Society for Rock Mechanics 1978). For instance, if a bedding plane is studied by 3D datasets, a  $0.1 \times 0.1$  m sample window could provide a good approximation to a plane in terms of its root-mean-square error (RMSE). However, if the sample window is  $100 \times 100$  m, the approximation of this surface to a plane could be poor, with a high RMSE. Another source of non-planarity in discontinuities is found in the termination of fractures, such as the “horsetail splay” (Vaskou 2016). Although few studies used digital datasets to investigate folded geological layers (Humair et al. 2015), it is usual to consider discontinuities as planes for practical purposes.

It is convenient to distinguish between three types of persistence when investigating rock masses: (a) visible persistence, or persistence extracted from visible data on rocky outcrops (i.e., only visible traces or exposed patches can be used), (b) real persistence, or persistence of the discontinuity within the rock mass (can only be investigated if combining geophysics or boreholes and visible data), and finally (c) estimated persistence, determined from information on

**Table 1** Parameters used to characterize discontinuities and methods of data collection (1978 and current)

Parameter	Traditional method (International Society for Rock Mechanics 1978)	Current methods
1. Orientation	(A) Compass and clinometer method Compass and clinometer Clino-rule of 50 m (B) Photogrammetric method Reconnaissance survey equipment Phototheodolite and tripod Control survey equipment Stereoscopic plotting instrument	3D point clouds 3D laser scanning (Jaboyedoff et al. 2012; Riquelme et al. 2014) Digital stereo-photogrammetry (Haneberg 2008; Lato et al. 2012) SfM (Jordá Bordehore et al. 2017)
2. Spacing	Measuring tape, min 3 m Compass and clinometer	3D point clouds TLS and ALS (Slob et al. 2010; Oppikofer et al. 2011; Riquelme et al. 2015)
3. Persistence	Measuring tape, min 10 m	3D point clouds TLS (Sturzenegger and Stead 2009a; Oppikofer et al. 2011)
4. Roughness	(A) linear profiling method and JRC (Barton and Choubey 1977) Folding straight edge of at least 2 m, in mm Compass and clinometer 10 m of light wire, marks at 1 m (B) Compass and disc-clinometer method Clar geological compass Four thin circular plates (C) Photogrammetric method: same as (1)	3D point clouds (Rahman et al. 2006; Haneberg 2007; Oppikofer et al. 2009; Khoshelham et al. 2011; Lai et al. 2014) Photographs (Alameda 2014) Profiles (Tatone and Grasselli 2010)
5. Wall strength	Geological hammer with one tapered end Strong pen knife Schmidt hammer: JCS Facilities for measuring the dry density of the rock	
6. Aperture	Measuring tape of at least 3 m, graduated in mm Feeler gauge White spray paint Equipment for washing the exposed rock	Infill scale-independent classification (Ortega et al. 2006)
7. Filling	Measuring tape of at least 3 m, graduated in mm Folding straight -edge, at least 2 m Plastic bags for taking samples Geological hammer with one tapered end Strong pen knife	Hyperspectral imaging (Kurz et al. 2011)
8. Seepage	Visual observation Air photographs, weather records	TLS (Sturzenegger et al. 2007; Vivas et al. 2015) Photographs Digital Photogrammetry Thermal images (Vivas et al. 2015)
9. N of sets	Based on (1)	Based on (1)
10. Block size	Measuring tape of at least 3 m, graduated in mm	3D point clouds TLS (Sturzenegger et al. 2011) SfM (Ruiz-Carulla et al. 2017)

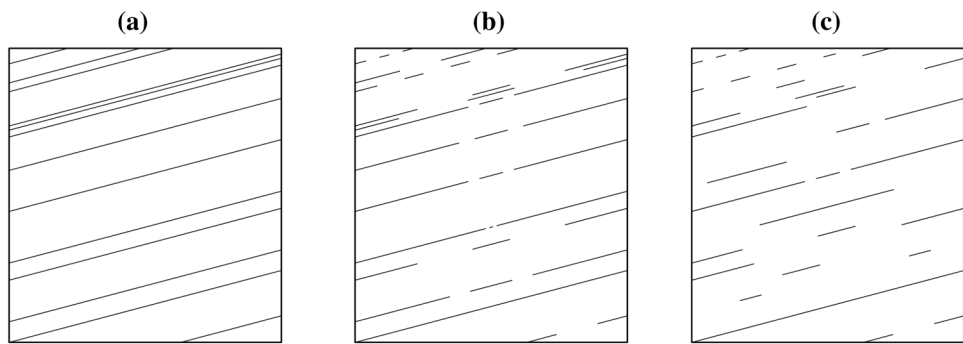
the surface of the rock mass. The work presented herein addresses estimated persistence, which is calculated considering that some superficial characteristics (i.e., orientation, spacing, persistence and roughness) are also present inside the rock mass.

The study of the discontinuity persistence parameter requires the classification of discontinuities as persistent (Fig. 1a), non-persistent (produced by intermittent discontinuities) (Fig. 1b) or as separate non-persistent discontinuities (Fig. 1c) (Hudson and Priest 1983). Other authors have considered the existence of macro-discontinuities persisting

to depths of thousands of metres (Goodman 1989). Persistent discontinuities could be affected by faults, reducing lateral continuity.

Analysis of persistent discontinuities is straightforward for 1D, 2D and even 3D measurements. Nevertheless, computation of the apparent lack of persistence produced by intermittent or separate discontinuities is not always a simple task. Mauldon (1994) suggested that intermittent non-persistent discontinuities are geologically unlikely, concluding in an implication of the existence of weakness planes throughout the rock mass, locally separated to form

**Fig. 1** Types of persistence produced by different persistent or non-persistent discontinuities: **a** persistent discontinuities; **b** intermittent discontinuity planes and **c** separate non-persistent discontinuity planes. Modified from (Hudson and Priest 1983)



discontinuities. Consequently, he suggested considering the intermittent discontinuities as persistent for mechanical analysis purposes (i.e., when a discontinuity plane is detected, coplanar discontinuity planes should be found and merged to calculate the persistence). Additionally, Mauldon (1994) concluded that although discontinuity intensity cannot be directly measured in an opaque rock mass, it can be estimated from outcrops (exposed areas) and line samples (boreholes and scanlines). Further studies have analysed the persistence within opaque rocks through the application of ground-penetrating radar (GPR) (Longoni et al. 2012).

Computation of discontinuity spacings from 3D point clouds has rapidly evolved during the most recent decade: Slob et al. (2010) considered discontinuities as persistent and measured the spacing with a virtual scanline, and Riquelme et al. (2015) considered both persistence and impersistence, assuming that the planes of a discontinuity set are parallel and proposed a method to measure the normal spacing for persistent and non-persistent discontinuities with 3D datasets, enabling the study and discussion on how to extract persistence information from 3D datasets.

A common situation in rock mechanics is incomplete information on the rock mass, hampering the investigation on discontinuity persistence of rock masses. A 3D dataset could exhibit intermittent discontinuity planes due to: (1) lack of discontinuities (e.g., there is a rock bridge and the discontinuity is really intermittent); or (2) impossibility of data collection due to occlusion (e.g., a rock was lying on the discontinuity and could not be scanned) or absence (e.g., the block defined by that part of the discontinuity slid down the slope or was removed). Traditional methods oversimplified the estimation of the “true” persistence by measuring the “visible persistence” (Sturzenegger and Stead 2009b; Oppikofer et al. 2011; Tuckey and Stead 2016), and therefore, there is still no method to estimate the real value of discontinuity persistence. The work presented herein proposes a methodology for the automatic mapping of the persistence of discontinuity sets on rock masses, using 3D datasets.

A component of the present study is based on previous findings for extracting discontinuity sets and clusters (i.e., sets of member points of the same plane) from 3D point

clouds (Riquelme et al. 2014, 2015). A new methodology is proposed herein to measure persistence from a geometrical perspective, using 3D datasets acquired by means of remote sensing techniques.

## 1.2 Measuring Persistence

Persistence was defined by the ISRM (1978) as the “areal extent or size of a discontinuity along a plane”. The same parameter was defined by Mauldon (1994) as the “measure of the degree to which discontinuities persist before terminating in solid rock or against other discontinuities”. The measurement of discontinuity persistence was initially proposed by computing the lengths in the direction of the dip and strike (International Society for Rock Mechanics 1978). Nevertheless, new available data can help develop new approaches to quantify the properties of discontinuities in a more realistic manner. Not surprisingly, true persistence is still considered difficult to be measured in practice (Shang et al. 2017), and therefore, actual persistence seems to be impossible to be measured using data acquired from the surface. Only visible persistence can be measured when using field data (regardless of the use of geophysics). A good example is the construction of a tunnel: the maximum persistence is limited by the maximum length of the visible discontinuities recognized in the excavation front, and therefore, by the excavation diameter, height or span. Herein, the focus is on the measurable persistence, using visible data only.

Einstein et al. (1983) defined the discontinuity persistence  $K$ :

$$K = \lim_{A_R \rightarrow \infty} \frac{\sum a_{Ri}}{A_R}. \quad (1)$$

$R$  is the region of a plane, with  $A_R$  being its total area and  $a_{Ri}$  the area of the discontinuity  $i$  within region  $R$ . This definition uses areal measurements, but frequently only trace lengths can be observed.  $K$  should be considered as a random variable because of the uncertainty of the measured values. Equation 1 can be adapted to lengths (Einstein et al.

1983). Later, Park et al. (2005) suggested that since rock exposures are small and 2D, it is impossible to measure the discontinuity area accurately in a field survey, suggesting the use of trace lengths (1D) to estimate persistence.

Discontinuity intensity  $I$  is a different rock mass index (i.e., the quantity of discontinuities within a given rock mass) and is used to determine the effect of jointing on the mechanical and hydrological performance of jointed rock masses (Dershowitz 1985). The intensity index is defined as the number of discontinuities per unit area or volume, or total discontinuity trace length per unit area or total area of discontinuities per unit of rock volume (Dershowitz and Einstein 1988). Intensity can be considered in two dimensions as areal intensity or in three dimensions as volumetric intensity. The intensity index is defined using the number of traces or their length, with several definitions and methods available (Dershowitz 1985; Zhang and Einstein 2000). For instance, the volumetric intensity (P32) is defined as (Einstein et al. 1983; Dershowitz 1985):

$$I = \lim_{V \rightarrow \infty} \frac{\sum a_i}{V} \quad (2)$$

$a_i$  is the area of the  $i$ th discontinuity in a 3D region of volume  $V$ .

### 1.3 Measuring Persistence from 3D Point Clouds

Persistence measurements have traditionally been collected using manual methods. Collection of measurements has experienced rapid evolution since 3D datasets have become available. Previous studies of persistence estimation using 3D datasets (acquired 3D laser scanners and digital photogrammetry) have manually measured features using profiles, on which lengths were measured parallel to the probable sliding direction (Oppikofer et al. 2011). Baecher's Disk Model (Baecher 1983) assumes that discontinuities are circular and defines the diameter of those circular discontinuities as "equivalent trace length" (Sturzenegger and Stead 2009a, b). More recently, Tuckey and Stead (2016) presented improvements on remote sensing methods for mapping discontinuity persistence and rock bridges in slopes, and also analysed three rock slopes of open pit mines using digital photogrammetry, LiDAR and window mapping datasets. Tuckey and Stead (2016) estimated persistence using the length of the discontinuity traces measured in field window maps, along with manually mapped best-fit circles to 3D datasets, which enabled the diameter measurements of outcrops. However, a major source of error was found in remote sensing surveys due to limitations in image resolution. High-resolution images enable identification of small discontinuities, whereas low-resolution images can result in indistinguishable smaller features (Ortega et al. 2006;

Sturzenegger and Stead 2009a; Tuckey and Stead 2016). 3D datasets enable automated or supervised analysis of geometric features. Several algorithms have been proposed for the extraction of the number of discontinuity sets and orientations (Jaboyedoff et al. 2007; García-Sellés et al. 2011; Gigli and Casagli 2011; Vöge et al. 2013; Assali et al. 2016; Wang et al. 2017; Chen et al. 2017), classification of point clouds (Riquelme et al. 2014) and normal spacing analysis (Riquelme et al. 2015). However, persistence measurement presents wide margins for improvements and could benefit from the aid of new methodologies.

## 2 Methodology

### 2.1 Definition of a Discontinuity Set and Cluster

The proposed methodology starts with a previously analysed point cloud. Discontinuity sets are extracted, along with their corresponding main orientations, and for each discontinuity set the parallel planar surfaces of the rock surface (patches) are identified. Additionally, each point is classified according to its discontinuity set and the plane to which it belongs.

Before introducing this methodology, it is convenient to outline previous concepts by means of an example consisting of a point cloud for a cube scanned by terrestrial laser scanner (TLS) (Fig. 2a). The cube is analysed by the open-source software discontinuity set extractor (DSE), which utilizes the methodology of Riquelme et al. (2014, 2016). Three discontinuity sets were identified, as shown in Fig. 2b. For each discontinuity set, two parallel patches or planes are identified (the base of the cube was not scanned, and therefore, it does not appear in this analysis). Essentially, a discontinuity set is defined by those points whose assigned normal vectors have approximately the same orientation. Therefore, those points that are members of a discontinuity set and present an even spatial density can be considered preliminarily as members of a plane (Riquelme et al. 2014). These sets of points correspond to 'patches' and are herein referred to as clusters.

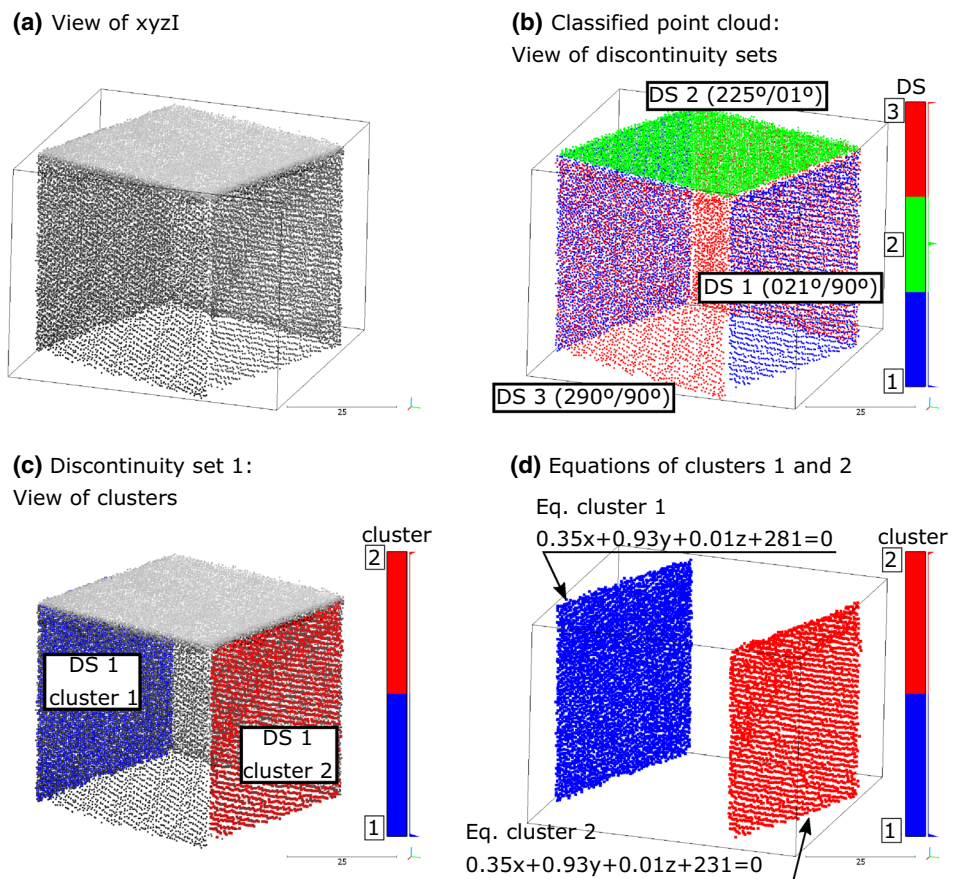
For DS 1 (Fig. 2b in blue), two planes or clusters are found as shown in Fig. 2c. Furthermore, the equations of both clusters are given by (Fig. 2c):

$$Ax + By + Cz + D = 0. \quad (3)$$

Both clusters present the same orientation [defined by the normal unit vector  $(A, B, C)$ ] but are non-coplanar because the constant parameter  $D$ , which represents the distance from the origin, is different (Fig. 2d).

In this work, the classified point cloud is defined by the following properties: coordinates of the points  $(x, y, z)$ , discontinuity set and cluster to which the point belongs to, and the parameters of the equation of the corresponding cluster  $(A, B, C, D)$ .

**Fig. 2** Classification of a TLS-derived point cloud cube: **a** 3D view of the point cloud; **b** view of the three discontinuity sets; **c** sets of member points (clusters) of the discontinuity set 1 that define two planes; and **d** equations of the planes of the two clusters of points shown in **c**. (Colour figure online)



## 2.2 Analysis of the Coplanarity of Clusters

In fieldwork, two planes can be considered coplanar after visual inspection and the assistance of traces. However, when this test is programmed using 3D datasets it is necessary to use a mathematical criterion to determine coplanarity. A simple case in which two horizontal planes are scanned using TLS is shown in Fig. 3a. Both planes are identified by two clusters of points: 1 and 2. A front view is shown in Fig. 3b, where coplanarity can be visually determined. However, elevations are represented in Fig. 3c, and the means of these elevations are 1.5486 and 1.5494 for clusters 1 and 2, respectively. As both means are slightly different, coplanarity cannot be definitively established.

In general, two planar clusters can be assumed to be coplanar when Eq. (4) is satisfied (Riquelme et al. 2015):

$$k \times (\sigma_1 + \sigma_2) \geq |D_1 - D_2|. \quad (4)$$

$D_1$  and  $D_2$  are the parameters of clusters 1 and 2, respectively,  $\sigma_1$  and  $\sigma_2$  are the standard deviation of the normal distances of all points to the best-fit-plane, and  $k$  is a parameter that controls the sensitivity of this test. This test can only be applied if all fitted planes have the same orientation, and therefore, the same parameters  $A$ ,  $B$  and  $C$  in Eq. (3).

In the example shown in Fig. 3c,  $D$  is equal to the mean of elevations because planes are horizontal. Otherwise, the least-square method should be used to calculate  $D$ . Then, if  $k$  is set to 3, the relationship shown in Eq. (4) is fulfilled as illustrated by Eqs. (5) and (6). Consequently, both clusters can be considered coplanar:

$$3 \times (0.00127 + 0.00118) \geq |-1.5483 - (-1.5494)|, \quad (5)$$

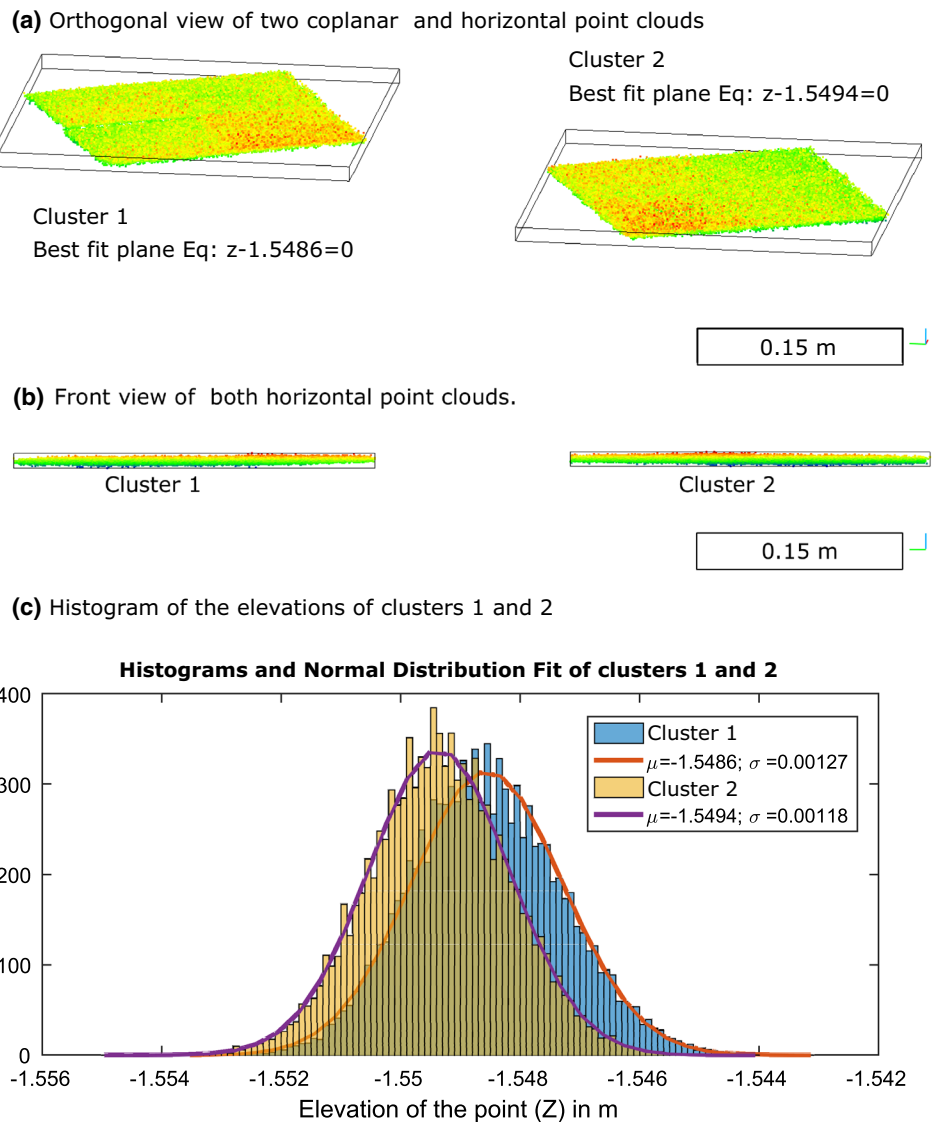
$$0.00735 \geq 0.0011. \quad (6)$$

In terms of rock mechanics, this means that the two analysed patches belong to the same discontinuity plane. If  $k$  is set to 0, all clusters of the same discontinuity set will be considered as different planes.

## 2.3 Computing Discontinuity Persistence

The proposed methodology starts by classifying an input dataset (3D point cloud) with the mean orientation of the discontinuity sets. Then, the algorithm analyses the clusters of member points of a given discontinuity set and searches for clusters that are coplanar within a certain user-supervised threshold controlled by parameter  $k$  from Eq. (4). Accordingly, the user must decide whether

**Fig. 3** Process of merging coplanar clusters of points, example of horizontal planes: **a** view of clusters 1 and 2; **b** front view of both clusters, that seem to be coplanar; **c** distribution of the z coordinates for each cluster



discontinuities will be considered as persistent or non-persistent (intermittent or separate, as presented in Fig. 1). When intermittent discontinuities are considered, the user must then decide whether empty areas between coplanar clusters are considered as: (a) non-scanned surfaces of a discontinuity (when detected patches should be merged); (b) rock bridges (when patches may or not be merged); or (c) simply rock (when they should not be merged). When a rock bridge is detected, the idea of establishing a threshold may emerge. This leads to considering the full area of all coplanar clusters (being conservative) when the size of the rock bridge is small, or measuring persistence as separate clusters when the rock bridge size is higher. However, the use of scanned data implies in uncertainties associated with the non-scanned rock mass. Therefore, the use of a threshold requires significant experience, meaning that this step requires careful consideration. Rock bridge

length remains underexplored in scientific literature, and therefore, further research is required.

Herein, Mauldon (1994) is followed despite the existence of rock bridges, if intermittent discontinuities are detected as coplanar, they are considered as a single merged discontinuity. This idea leads to higher values for persistence, and is more conservative.

A flowchart of the proposed methodology for the calculation of discontinuity persistence is shown in Fig. 4. The first stage consists of the analysis of the coplanarity of clusters for every discontinuity set. This process estimates if two or more clusters are coplanar as defined in Sect. 2.2 and modifies the parameter  $D$  of the corresponding plane. The next step consists of merging separate clusters with the same parameter  $D$  into a single cluster.

The second stage consists of the measurement of the persistence. The member points of each discontinuity set

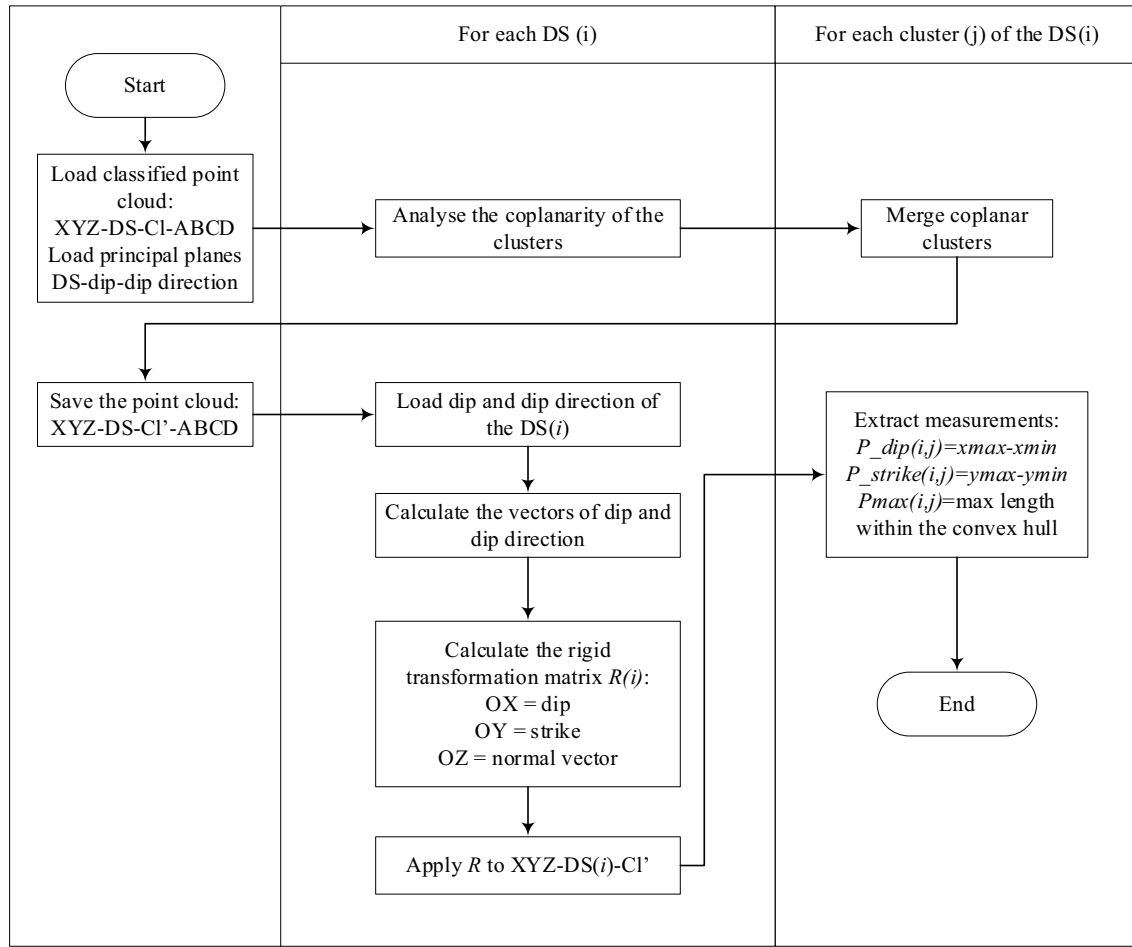


**Fig. 4** Workflow of the proposed methodology

are extracted, and a transformation is applied using a rigid transformation matrix  $\mathbf{R}$ :

$$\mathbf{R} = \begin{bmatrix} \cos(\beta) \sin(\alpha) & -\cos(\alpha) \sin(\beta) \sin(\alpha) \\ \cos(\beta) \cos(\alpha) & \sin(\alpha) \sin(\beta) \cos(\alpha) \\ -\sin(\beta) & 0 & \cos(\beta) \end{bmatrix}. \quad (7)$$

In this matrix  $\beta$  and  $\alpha$  are the dip and dip direction angles of the corresponding orientation of the discontinuity set, respectively. Alternatively, this transformation can be applied to each cluster whose centroid has been previously translated to the origin of the coordinate system.

Figure 5 shows a scheme of the transformation, which enables the direct extraction of the maximum discontinuity persistence measured in the directions of the dip and strike, according to ISRM (1978). Considering the set of points  $X(i, j)$ , members of the discontinuity set id  $i$  and simultaneously of the cluster of points id  $j$ , Eqs. (8) and (9) show how both lengths are calculated, where  $x'(i, j)$  and  $y'(i, j)$  are the local coordinates of  $X(i, j)$ :

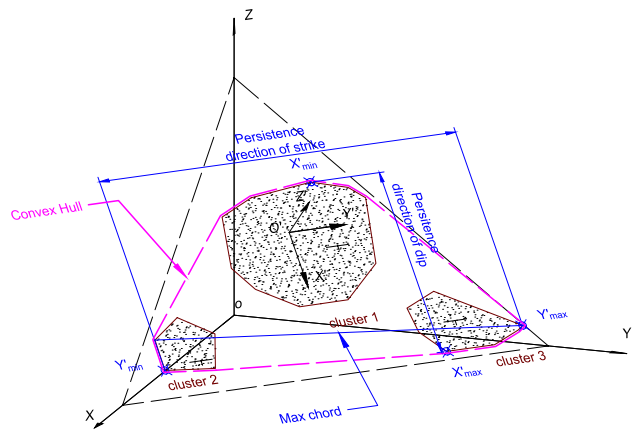


**Fig. 5** Perspective of the 3D point cloud for three patches of a discontinuity. Three clusters are identified as coplanar and the convex hull is extracted. A coordinate system transformation is applied, where OXYZ is the original and O'X'Y'Z' the transformed. Persistence is extracted in the direction of dip O'X' and in the direction of strike O'Y'. O'Z' is orthogonal to plane O'X'Y' and has the direction of the normal vector of the plane

$$\text{Length - Persistence}_{\text{dip}}(i,j) = \max(x'^{(i,j)}) - \min(x'(i,j)), \quad (8)$$

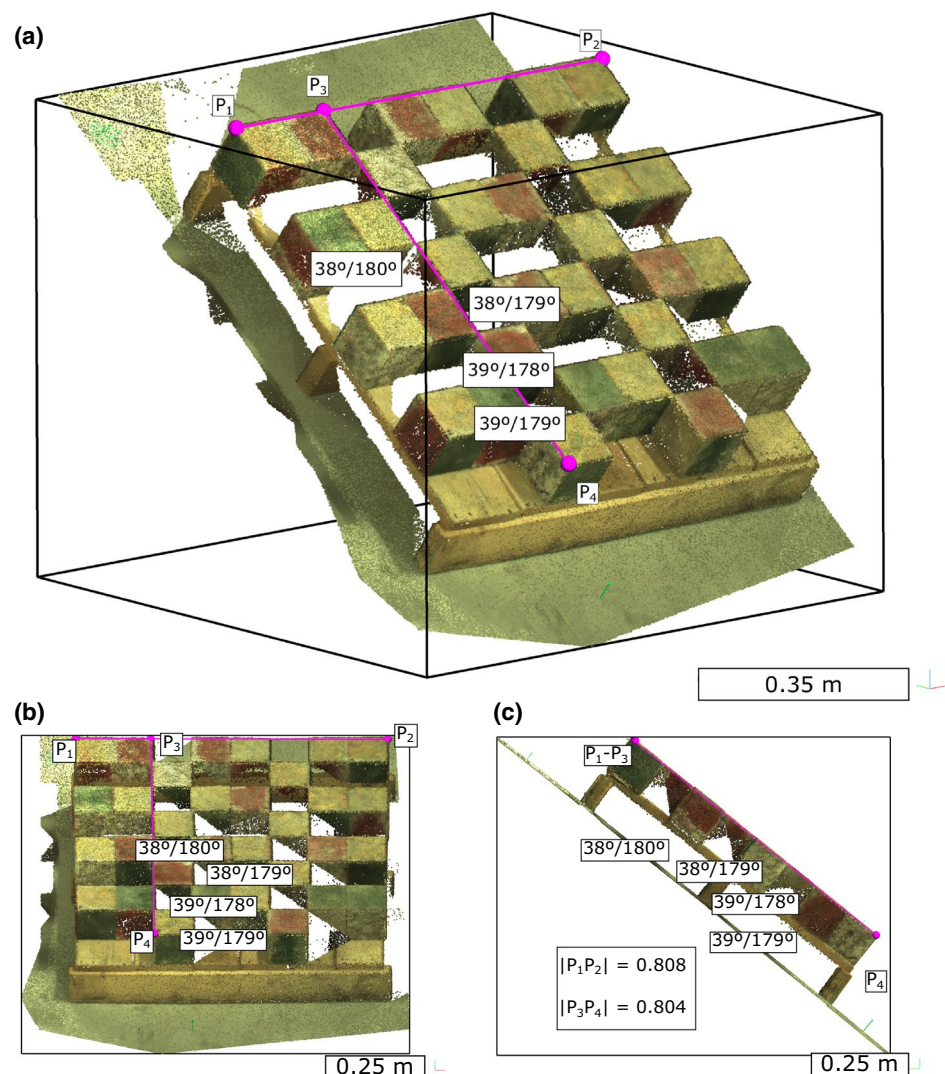
$$\text{Length - Persistence}_{\text{strike}}(i,j) = \max(y'^{(i,j)}) - \min(y'(i,j)). \quad (9)$$

Additionally, the maximum length can be calculated through the computation of the convex hull  $C_h(X(i,j))$  according to Eq. (10). The convex hull also enables the estimation of the area of the cluster according to Eq. (11). The convex hull is calculated by the projection of the cluster points on the  $OXY'$  plane, and then function ‘convhull’ (available in MATLAB software) is applied, which returns the convex hull of points  $X(i,j)$ .

$$\text{Length - Persistence}_{\text{max}}(i,j) = \max \text{length}(C_h(X(i,j))) \quad (10)$$

$$\text{Area - Persistence}(i,j) = \text{Area}(C_h(X(i,j))). \quad (11)$$

**Fig. 6** Case study 1: a laboratory model. **a** Orthogonal 3D view of the cubes; **b** front view of the cubes and **c** side view of the cubes. Shadow areas exist due to the scanning process. (Colour figure online)



### 3 Case Study

#### 3.1 Case Study 1

The first case study consists of a laboratory test where regular cubes of granite are organised on a pallet that lies on the floor (Fig. 6). The side of each cube is approximately 0.095 m. The granite cubes are arranged forming a square, whose side is approximately 0.8 m (distances  $|P_1P_2|$  and  $|P_3P_4|$  in Fig. 6). This setup was scanned by a TLS model Leica C10 from three stations, and registered using high-definition surveying (HDS) targets by means of the Leica Cyclone software (Leica 2016). Finally, the 3D point cloud was rotated to represent a non-horizontal discontinuity.

Three orthogonal discontinuity sets are used in this case study. The top of the set of cubes represents a planar discontinuity. Empty spaces between cubes (i.e., deleted cubes)

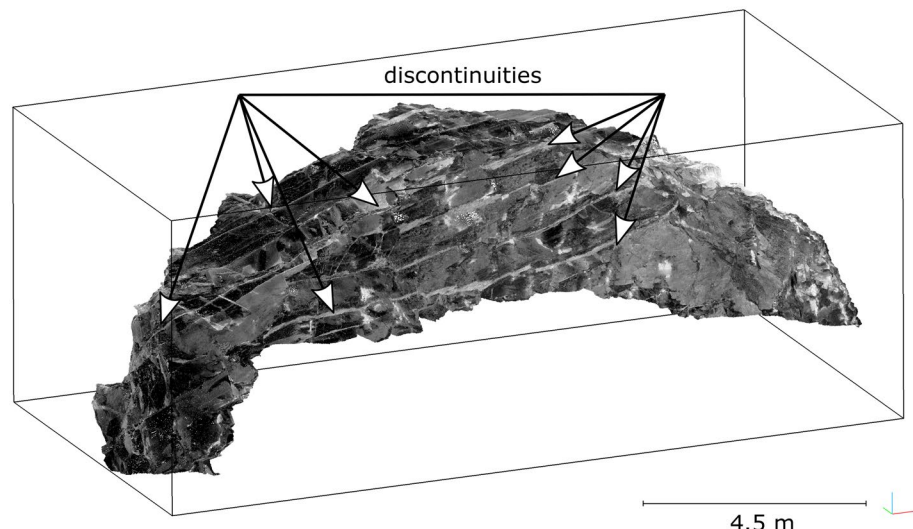
represent rock bridges (which cannot be scanned) or discontinuities that are hidden within the rock or simply not present. The dip angle of this discontinuity is  $39^\circ$  and dip direction is  $180^\circ$ . Additionally, some of the cubes have been randomly removed to represent intermittent discontinuities. As a result, there are clusters of points with the same orientation and that belong to the same discontinuity set. Two more sub-vertical discontinuity sets are present on the sides of the cubes. This case study will be used to validate the proposed methodology.

### 3.2 Case Study 2

This case study aims to apply the proposed methodology to a real cavern rock surface. A 3D point cloud was downloaded from a public repository (Lato et al. 2013) to allow reproducibility. It consists of a cavern excavated in weathered gneiss in Oslo (Norway), in 2011. The surface of the cavern was scanned using a phase-based Faro Photon 120 and two scan stations (acquisition of two point clouds), with a point spacing of less than 1 cm (Fig. 7).

The surface of the cavern shows three differentiated regions: shotcrete, planar outcrops of rock and rock damaged during the blasting process. Only planar outcrops of intact rock are of interest, so shotcrete and damaged rock areas were cropped from the available 3D point cloud. Case study 2 provides a real case scenario with a discontinuity set that can be identified on both sides of an excavation. Therefore, the proposed methodology should be able to identify separated patches of the same discontinuity and measure the persistence of separated clusters of points of the same discontinuity. Manual measurements were made and compared with those derived from the 3D point clouds to validate the results.

**Fig. 7** Case study 2: a cavern in Oslo downloaded from the Rockbench Repository (Lato et al. 2013), with a selected surface for analysis



### 3.3 Case Study 3

Case study 3 consists of a carbonate flysch rock slope over a railway tunnel protection track (Fig. 8a–c) (Cano and Tomás 2013). The bedding plane is observed as a persistent sub-vertical discontinuity set, which presents some waviness (Fig. 8c). One scan station was performed using a long-range 3D laser scanner model Optech at 200 m. The 3D point cloud was registered to a levelled DEM (not oriented with respect to the north), so dip measurements could be extracted. The point cloud was decimated with a spacing of 0.1 m, yielding an evenly spaced point cloud.

This case study aims to demonstrate the proposed methodology using typical rock slope problems and scans conducted at longer ranges than previous case studies. As the discontinuity is persistent, measurements using the 3D point cloud should provide results according to the sample window size (i.e.,  $40 \times 25 \times 25$  m).

## 4 Results

### 4.1 Case Study 1

The methodology requires the classification of the point cloud to differentiate the discontinuity set and, subsequently, the cluster of points. Three discontinuity sets were found (Fig. 9a, b). Consequently, the clusters of points were extracted (Fig. 9c, g). The orientation of discontinuity set 1 is ( $179^\circ/39^\circ$ ), as expected, and corresponds to the top of the cubes. As all cubes are distributed contiguously, a single cluster of points is detected for this discontinuity set (Fig. 9c). The orientations of discontinuity sets 2 and 3 are ( $359^\circ/51^\circ$ ) and ( $089^\circ/89^\circ$ ), respectively. The clusters of points extracted are not contiguous, and are identified as

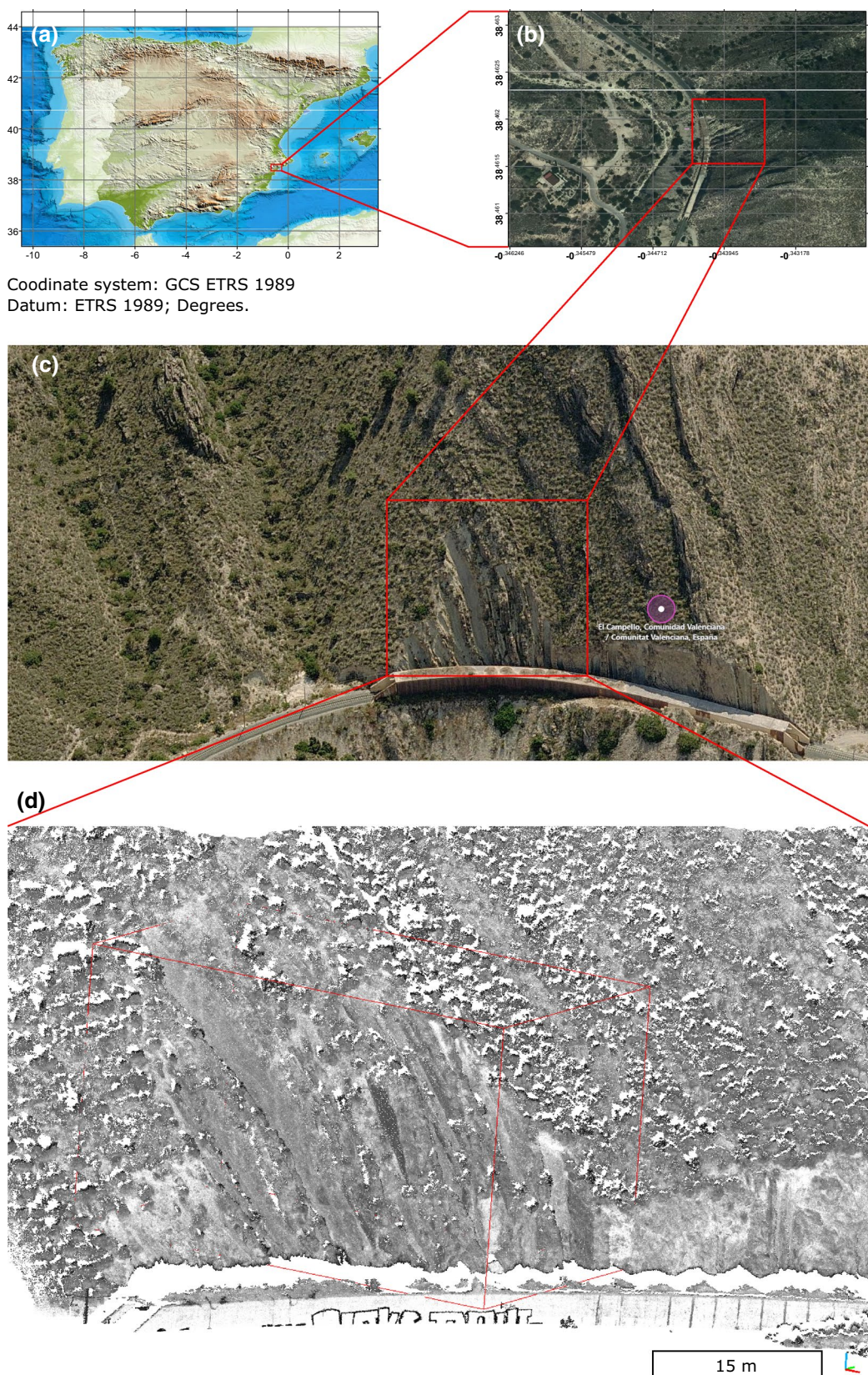


**Fig. 8** Case study 3: carbonate flysch outcrop in El Campello, Spain: **a, b** location of the rocky slope; **c** aerial image of the rock; **d** 3D point cloud scanned using a long-range 3D laser scanner. (Colour figure online)

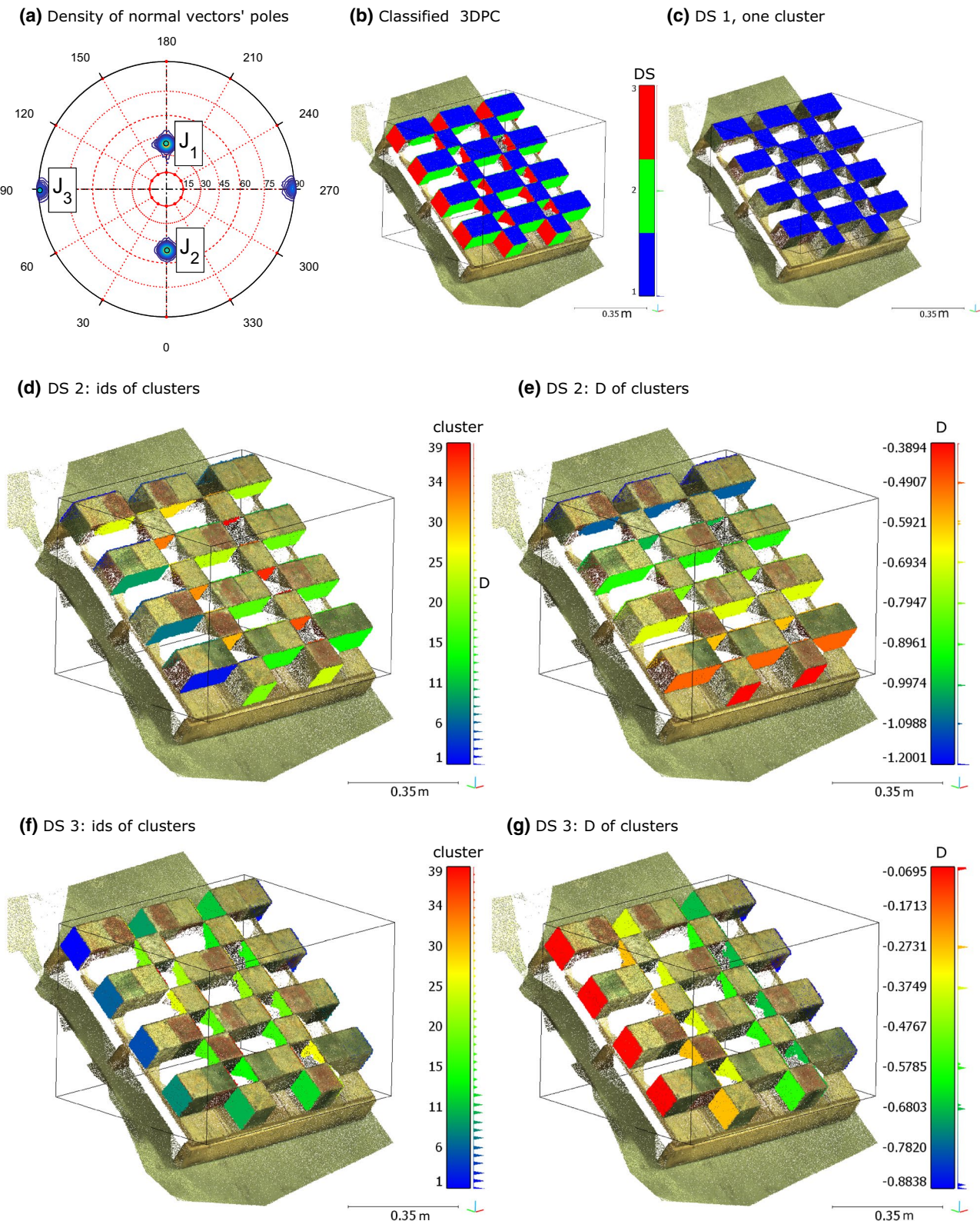


**Fig. 9** Results of case study 1: **a** density of the poles of the normal vectors; **b** classified point cloud; **c, d** and **f** clusters of DS 1, 2 and 3, respectively; **e, g** clusters of DS 2 and 3, respectively, classified according to parameter  $D$ . (Colour figure online)

different (Fig. 9d and f). However, coplanar clusters were merged after the analysis to determine if they were coplanar or not (Fig. 9e and g). Merging coplanar clusters considered that parameter  $k$  of Eq. (4) was 3.

The proposed methodology calculates the persistence of those clusters that have the same  $D$  parameter, or in other words, are considered to belong to the same discontinuity. The single cluster for discontinuity set 1 is shown in Fig. 10a. The convex hull of the cluster is represented as a closed polygon filled in transparent red. This point cloud has been transformed to a new local coordinate system in which the measurement of the persistence can be performed.

A more complex scenario was obtained for discontinuity set 2, where clusters are identified separately (Fig. 9d) but coplanarity analysis has merged some clusters (Fig. 9e), e.g. cluster 2 (Fig. 10b). This leads to the measurement of the persistence as a continuous surface, instead of different isolated regions.

Discontinuity set 3 shows a case in which four clusters were expected to be coplanar, but are not. Four clusters can be seen on the left side of the cubes (Fig. 9f). However, the analysis merged those clusters not as a single set but as two different sets (Fig. 10c, d). Accordingly, parameter  $D$  for both sets shows a separation of approximately 6 mm. A subsequent detailed inspection of those clusters showed that those four sides were not as coplanar as initially supposed. This is due to the precision of rock cutting and manual placement. The standard deviation ( $\sigma$ ) of the point-plane distances of these clusters is approximately 0.85 mm (considerably flat surfaces). Considering Eq. (4) and  $k=3$ , if normal spacing between clusters is higher than 5 mm, the clusters are considered as different, and consequently persistence is not measured in the merged clusters. Although a persistence measurement of 0.8 m was expected, two measurements of 0.51 and 0.50 m were extracted. A possible solution to this issue is to increase the  $k$  value to 3.5.

For all discontinuity sets, the persistence was measured in the directions of dip and strike as well as the length of the maximum chord and the area of the convex hull. Measured persistence values were plotted in the corresponding histograms shown in Fig. 11. Additionally, a negative exponential distribution was plotted using the corresponding mean persistence or mean discontinuity trace length and the mean trace termination frequency ( $\lambda$ ) (Priest and Hudson 1981). It can be observed that the histograms do not fit properly to the assumed probability distribution. However, in this case study, the size of the sample is small (i.e., 1–10 samples), and the physical model is not a rock slope.

Case study 1 deepens understanding on the application of the proposed methodology and shows that the obtained persistence values correspond to the expected values. The length of the maximum chord within the convex hull is shown in Table 2, and the maximum length corresponds to

the size of the global set of cubes. In contrast, the observed mean value is less than the expected value. A possible explanation is that the merging of clusters is sensitive to irregularities: dividing a set of clusters into subsets (e.g., case of discontinuity set 3, clusters 1 and 6 of Fig. 10c, d) increases the size of the sample and reduces the measured persistence. Both facts lead to a reduction in the mean value, while the maximum remains invariant. Consequently, it seems appropriate to consider the persistence as the interval defined by the mean and the maximum values.

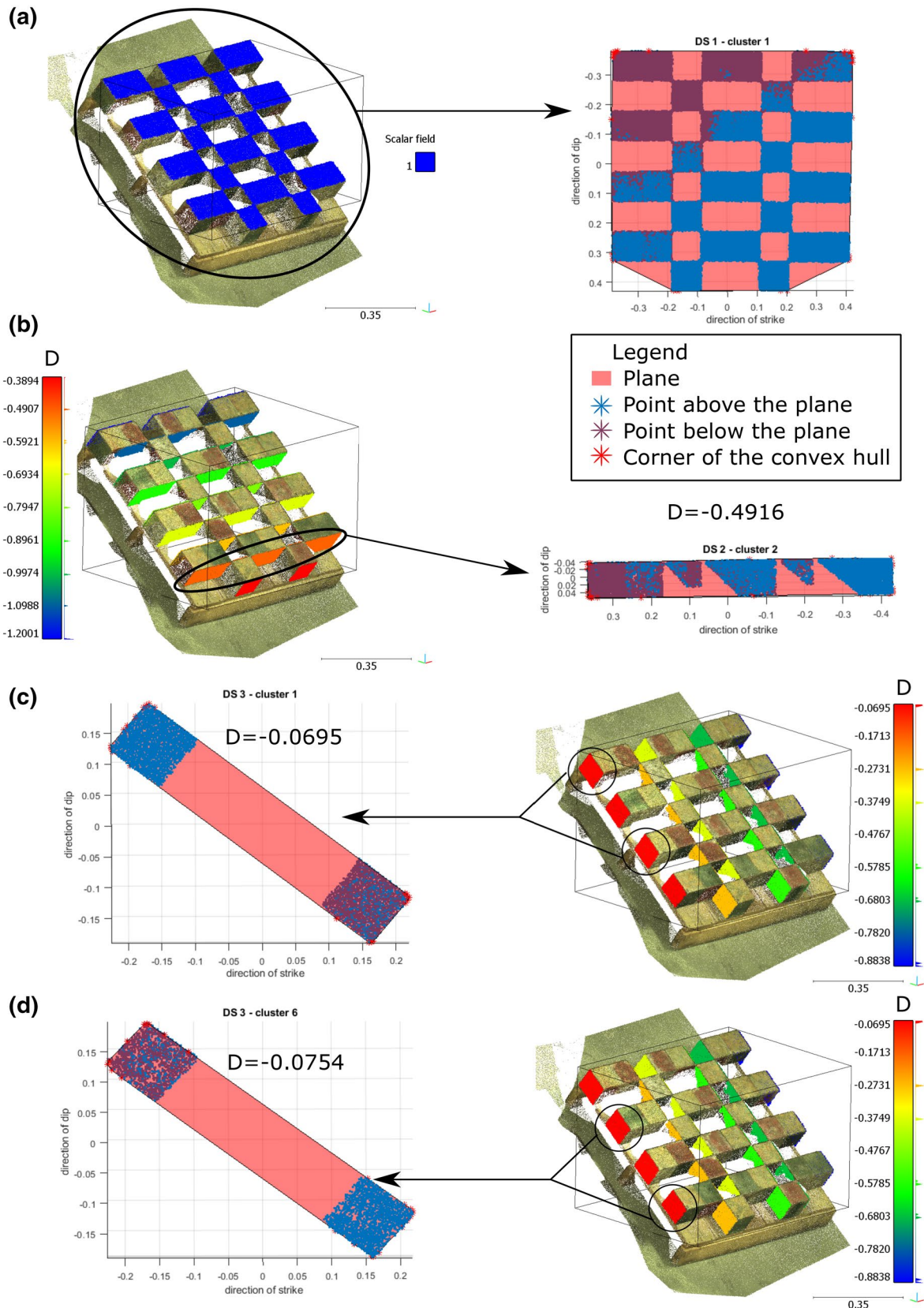
## 4.2 Case Study 2

For case study 2, the classification of the point cloud was initially performed using software DSE. The normal vector orientation of each point was calculated using 30 neighbours to enable higher convergence of the principal orientations (i.e., discontinuity set orientation). The value of tolerance (parameter utilized by software DSE) was set to 0.2 (Riquelme et al. 2014). The number of bins was set to 256 to represent the density of the poles of the normal vectors, enabling higher accuracy. The minimum angle between principal normal vectors was set to 30°. Assignment of a point to a principal pole considered that the minimum angle between the assigned normal vector of that point and the principal pole candidate was set to 15°. This value ensured that resulting planes were more planar and less irregular. For each cluster, the calculated plane fixed the orientation equal to the corresponding discontinuity set. This assumption resulted in all clusters that were members of a discontinuity set. Additionally, clusters were merged using  $k=3$  (4).

Five discontinuity sets were extracted based on the density of the poles (Fig. 12e). Visual inspection of the classified point cloud provided a planar pattern on the surface of the cavern (Fig. 12c, d). Additionally, the normal spacing was analysed using the methodology proposed by Riquelme et al. (2015), and implemented in the software DSE. The obtained values of the normal spacing for discontinuity set 1 were 0.35 m for the non-persistent hypothesis and 0.13 m for the persistent hypothesis.

As case study 2 corresponds to the surface of a convex cavern, it was interesting to determine whether or not a series of discontinuities located on the same plane (but not connected) could be successfully identified as a single discontinuity in a real scenario. A detailed example in which discontinuity set 1 has been analysed is shown in Fig. 13. The merged cluster numbers 6 and 10 (with  $D$  values  $-9.0250$  and  $-7.5093$ , respectively) have been extracted for illustration purposes (Fig. 13a, c, respectively).

The first discontinuity (i.e., discontinuity set 1, cluster 6,  $D=-9.025$ ) extends throughout almost the entire study area (Fig. 13a, b). Manually measured persistence ranges from



**◀Fig. 10** Results of case study 1: identification of some merged clusters of points. **a** DS 1 (blue) only shows a single cluster of points, result of merging of clusters of the top of the cubes; **b** DS 2, a set of coplanar clusters of the side of the cubes; **c, d** DS 3, two sets of clusters that were expected to be recognised as coplanar (left side), but due to the non-exact coplanar disposition of the cubes, were recognized as two different sets. (Colour figure online)

11 to 13 m. The proposed method indicates a maximum estimated persistence of 13.69 m. However, Fig. 13e shows that this discontinuity is curved, which results in patches of two adjacent discontinuities being identified as a single discontinuity. This indicates that if the scale of the study area is greater than the spacing of discontinuities, the natural curvature might lead to the mixing of discontinuity clusters. In this case, normal spacing is approximately 0.2 m and persistence is approximately 14 m. The ratio between the scale and the normal spacing is  $14/0.2 \approx 70$ .

The size of the second discontinuity is smaller than the first one (Fig. 13c, d). Manually measured persistence is approximately 8 m, and the proposed method indicates a maximum persistence of 8.44 m. In this case, visual inspection indicates that the clusters belong to the same discontinuity (Fig. 13e). The ratio between the scale and the

persistence is approximately  $8.44/0.2 \approx 40$ , almost half the value obtained in the previous case.

These results suggest that the probability of merging clusters incorrectly increases with: (1) larger study area sizes; (2) smaller extent of clusters; (3) higher waviness of the folding of discontinuities, and (4) smaller normal spacing of discontinuities.

Unlike case study 1, the number of measurements is higher in this case, and therefore, the histograms of persistence fit better to a negative exponential distribution (Fig. 14). Persistence values extracted from the maximum length of the convex hull are shown in Table 3. It must be mentioned that the expected values correspond to the maximum values and not to the mean values; this occurs because a number of small clusters are identified and provide low values of persistence. Therefore, it is appropriate to provide a range of persistence values rather than providing a single value or distribution.

The methodology has been applied to this case study considering parameter  $k=0$  (i.e., clusters are not merged and persistence is measured separately) to analyse the effect of merging clusters. Table 3 shows the measured persistence for this case. The observed persistence values

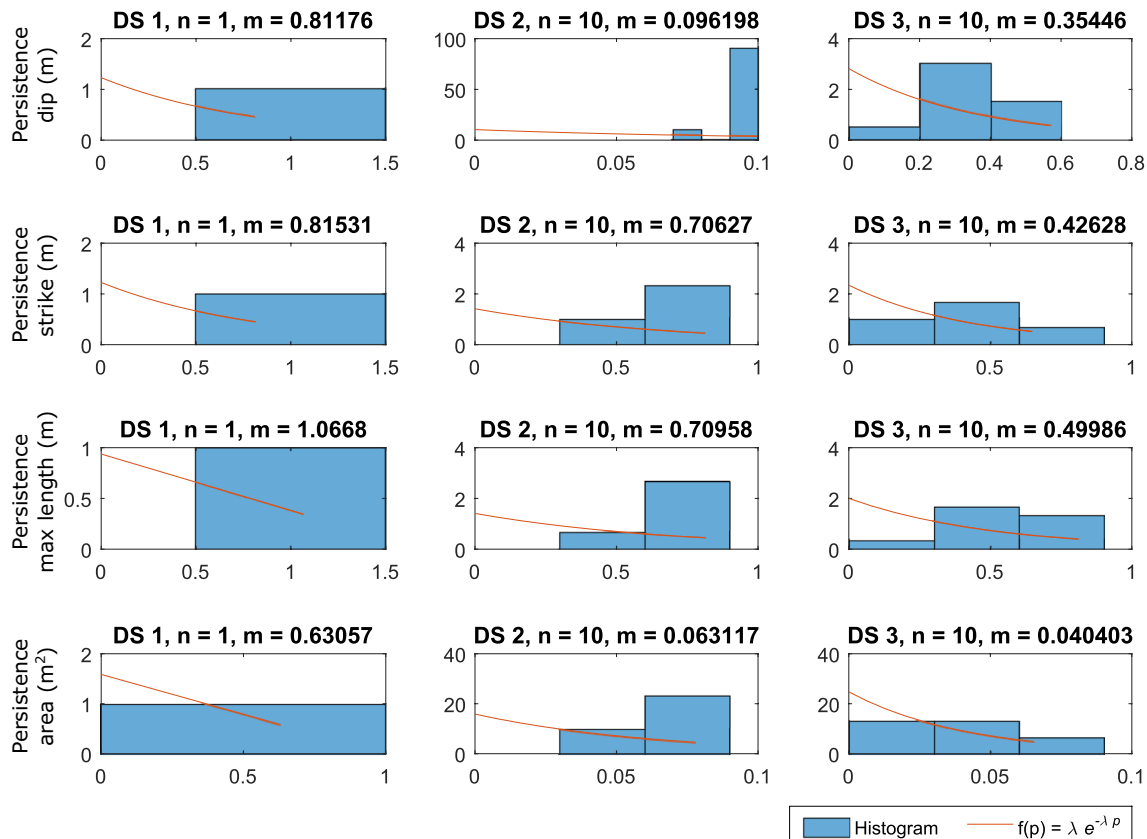


**Fig. 11** Case study 1. Histograms of the three defined discontinuity sets for persistence measured in the direction of dip, strike, maximum length within the convex hull and area

are lower than those calculated considering the merging of the clusters. Moreover, these values only consider the extent of single clusters, and the existence of coplanar discontinuities is not considered. Accordingly, the

observation of discontinuity set 1 shows that this assumption is inappropriate as the manually extracted value is higher (i.e., 14 m).

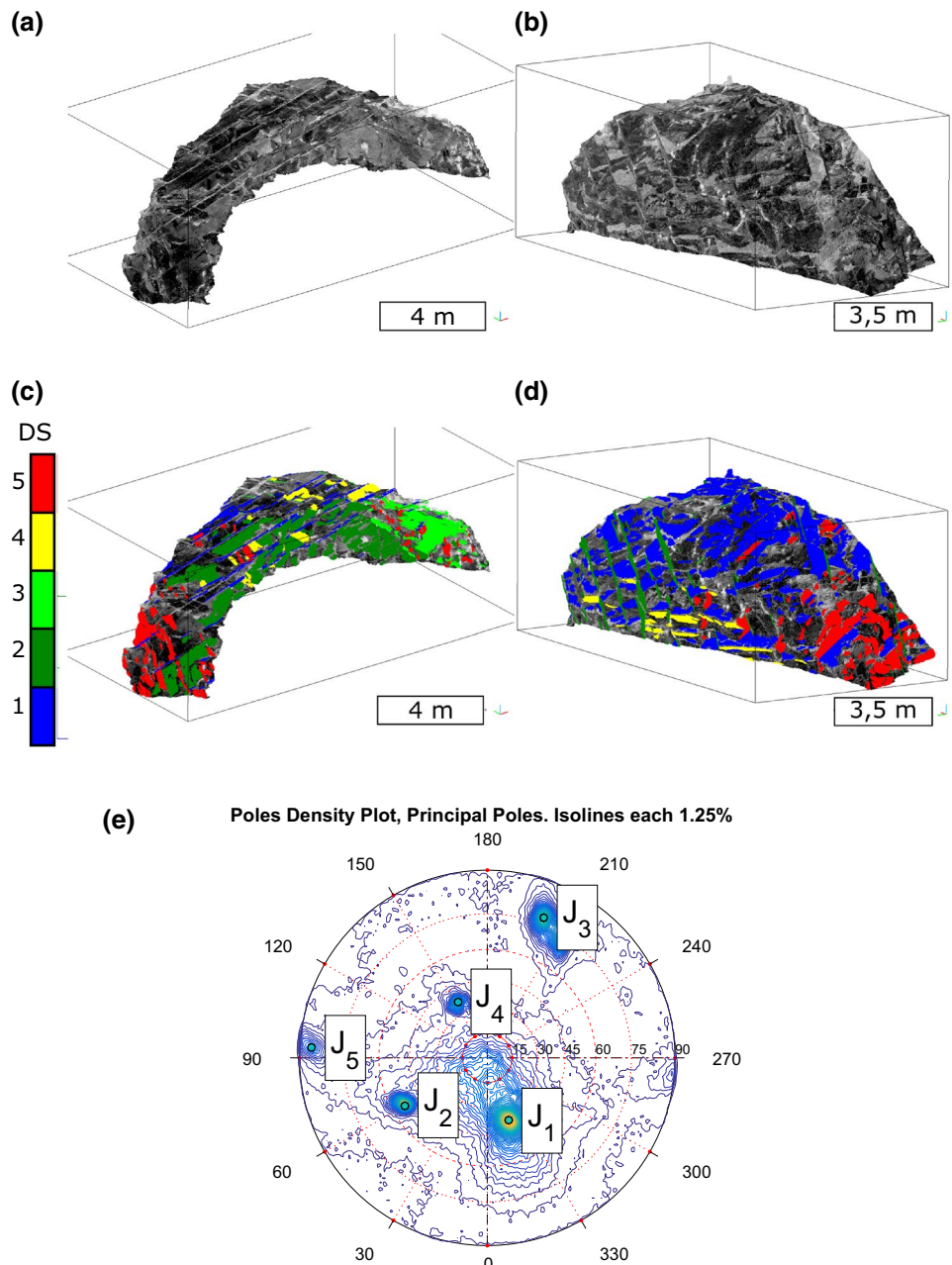
### 4.3 Case Study 3

First, the 3D point cloud was analysed using the DSE software. As a result, a sub-vertical discontinuity set was extracted ( $025^\circ/086^\circ$ ), which corresponded to the bedding plane (Fig. 15). Clusters with less than 50 points were removed, so the minimum size of clusters is  $0.5 \text{ m}^2$ . The normal spacing of this discontinuity set was analysed considering non-persistent

**Table 2** Case study 1: extracted persistence of DS 1

Persistence	Mean	Max	Expected
Dip (m)	0.8118	0.8118	0.80
Strike (m)	0.8153	0.8153	0.80
Maximum (m)	1.0668	1.0668	1.13
Area ( $\text{m}^2$ )	0.6306	0.6306	0.64

**Fig. 12** Case study 2. Classification of the point cloud in one colour per DS: **a, b** 3D orthogonal view of the unclassified point cloud and **c, d** respective classified point clouds; **e** density of poles of the extracted DS,  $J_1$  (342/39);  $J_2$  (060/54);  $J_3$  (202/78),  $J_4$  (152/37) and  $J_5$  (093/86). (Colour figure online)



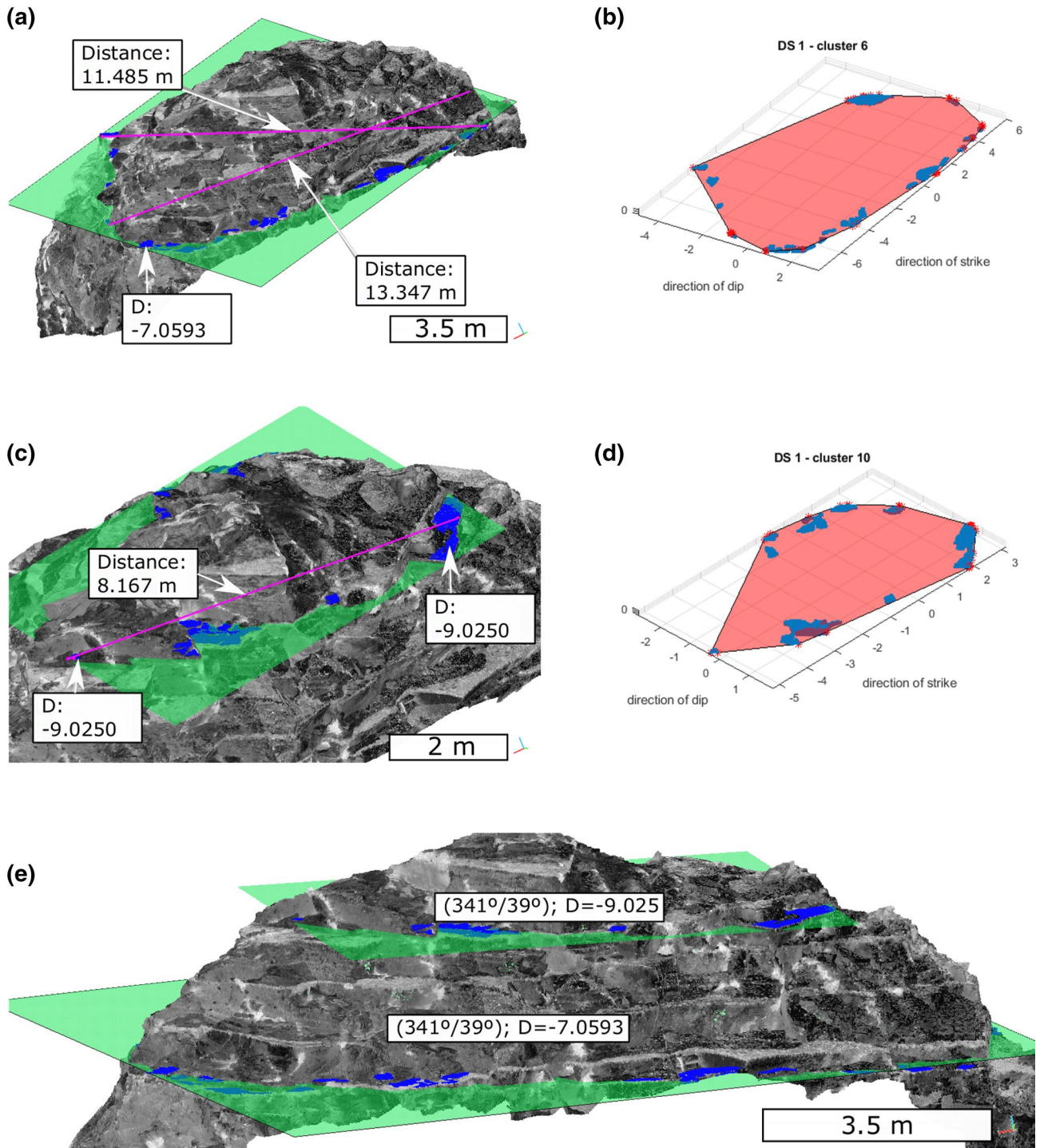


**Fig. 13** Case study 2. Extraction of the persistence of a discontinuity within DS 1,  $D = -9.025$ . **a** 3D orthogonal view of the point cloud and the extracted cluster members of the same plane; **b** member

points of the plane  $D = -9.025$  and its convex hull; **c, d** similarly to  $D = -7.5093$ ; **e** view of both estimated discontinuities. (Colour figure online)

and persistent discontinuities, providing mean values of 1.5 and 1.1 m, respectively. A mean normal spacing of 1.1 m was considered in the analysis of the persistence.

Measured discontinuity persistence is shown in Fig. 16. The average values in the direction of the strike and in the maximum direction are 8.0 and 11.7 m, respectively.

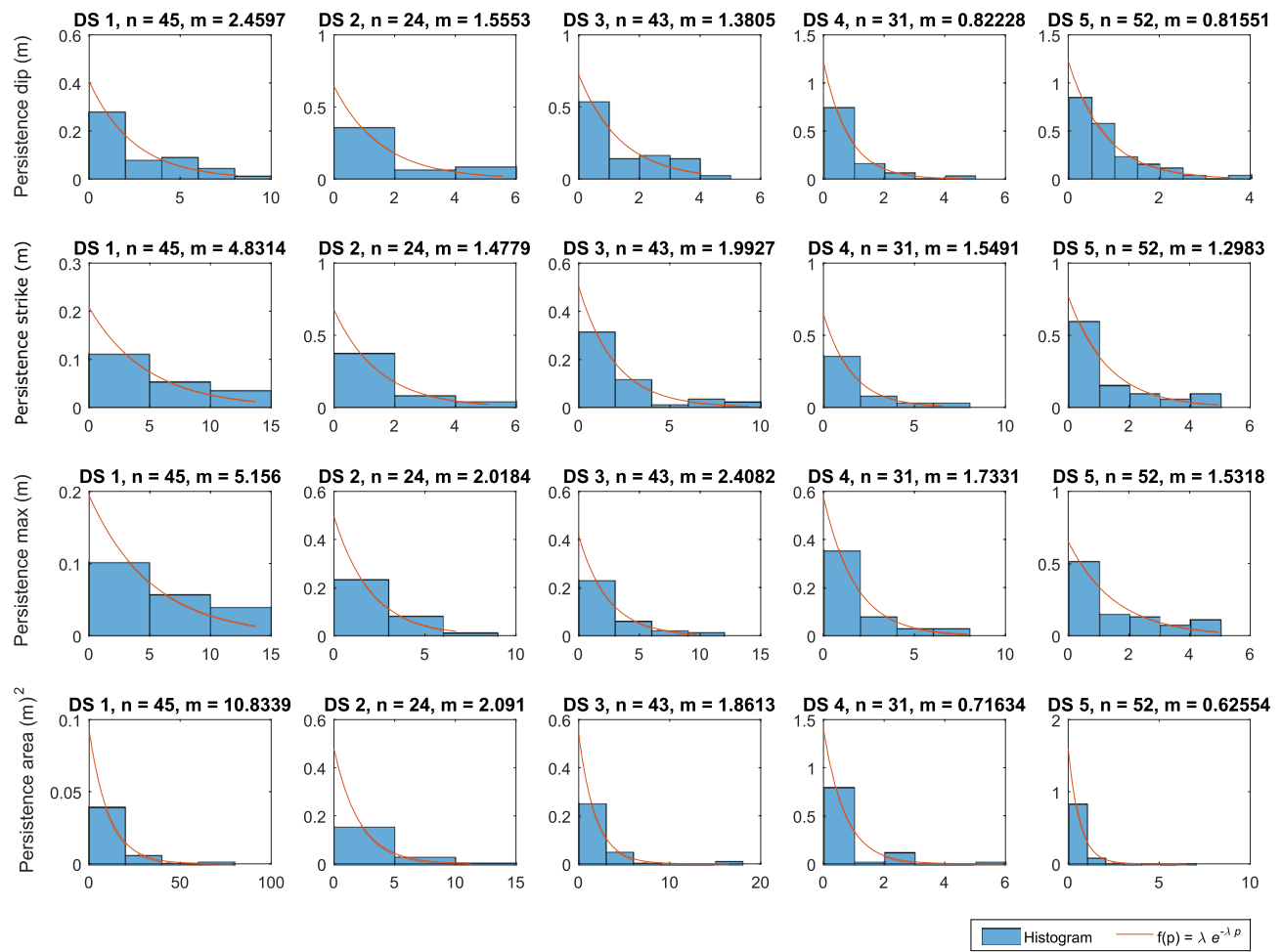


**Fig. 14** Case study 2. Histograms of the five defined discontinuity sets for persistence measured in the direction of dip, strike and maximum chord within the convex hull and the area of the convex hull

**Table 3** Case study 2: extracted persistence measured in the direction of maximum length

Discontinuity set	$k=3$		$k=0$	
	Mean (m)	Maximum (m)	Mean (m)	Maximum (m)
01	5.1560	13.6965	0.5084	3.0904
02	2.0184	6.7079	0.4291	3.7815
03	2.4082	9.7109	0.6799	3.0416
04	1.7331	7.9335	0.5225	2.2660
05	1.5318	4.9280	0.3788	2.2097

However, maximum values are 18.0 and 27.0 m, approximately. The maximum value is similar to the size of the sampling window.

## 5 Discussion

### 5.1 Discussion of the Analysed Case Studies

This work presents a novel methodology to semi-automatically analyse the persistence of discontinuity sets using 3D point clouds. The proposed approach build upon the ISRM method, applied to measure the persistence of discontinuities (International Society for Rock Mechanics 1978)—the method proposed herein has been further adapted to the acquisition of modern digital datasets to fully exploit 3D capabilities.

Three case studies have been utilized to illustrate the application and validate the proposed method. Case study 1 shows that the method successfully identifies sets or member points of the same plane and measures the persistence. Case study 1 consists of regular cubes whose sides represent exposed planes with the empty spaces corresponding to rock bridges or non-scanned planes. The method was able

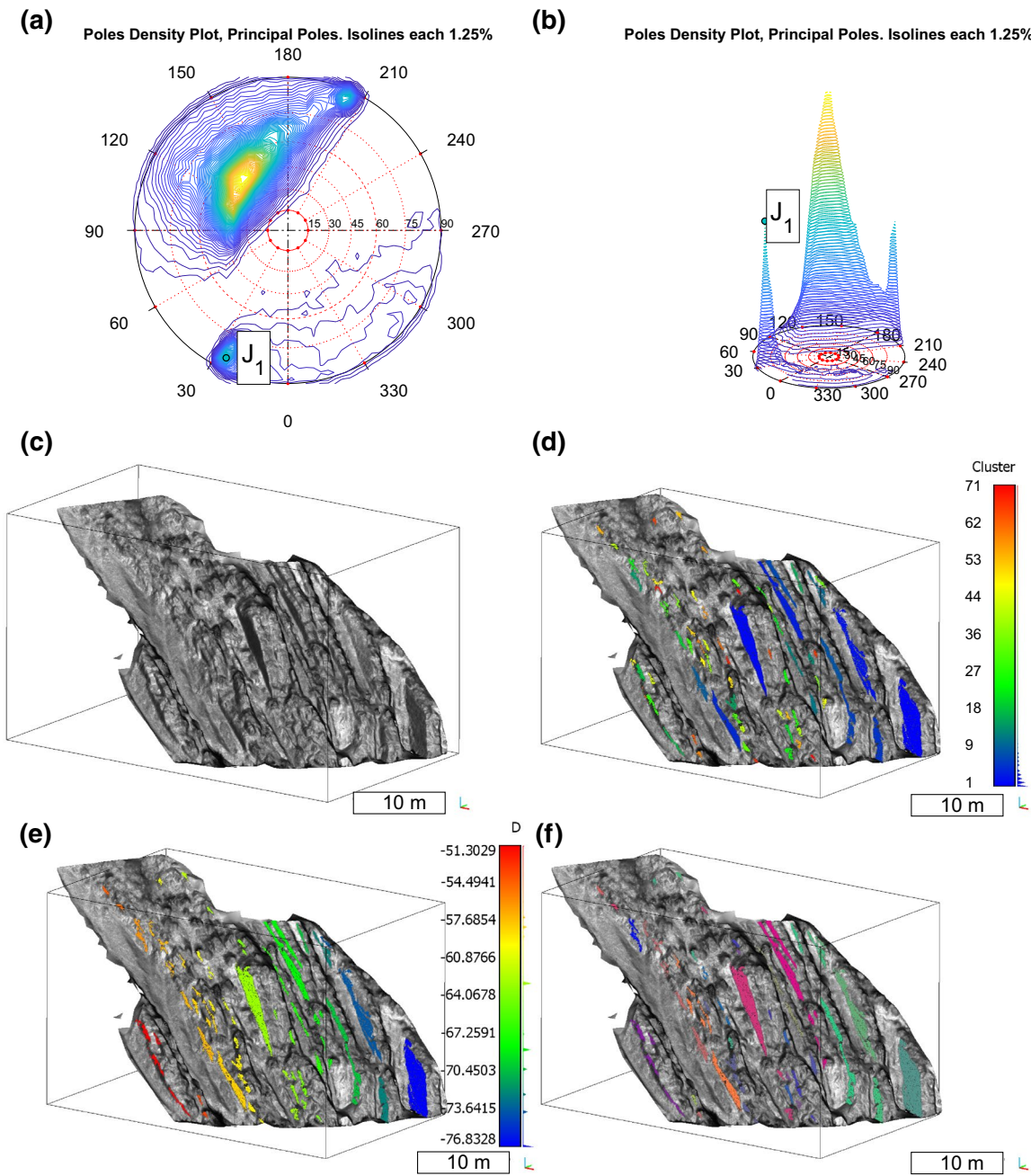


**Fig. 15** Case study 3. **a, b** Density of the poles of the normal vectors; **c** analysed sector; **d** clusters extracted from discontinuity set 1; **e** clusters classified according the value of  $D$  and **f** merged clusters grouped per randomized colours. (Colour figure online)

to merge coplanar clusters in some cases. However, other clusters were detected as different clusters. Interestingly, detailed analysis of data showed that these clusters were not as coplanar as expected. Therefore, this work highlights that discontinuities are not planes but surfaces that present roughness and waviness characteristics.

Case study 2 presents a cavern and demonstrated that the proposed methodology was able to successfully extract the persistence. The specific geometry (i.e., circular section)

enabled discontinuities to be scanned on both sides of the section, which proved to be useful for validating the method. Clusters of 3D points belonging to the same plane were successfully detected on both sides of the rock mass.

Case study 3 presents a carbonate flysch rock slope, scanned using a long-range 3D laser scanner at 200 m. Despite the waviness of the bedding plane, a number of clusters were successfully merged. Additionally, the largest

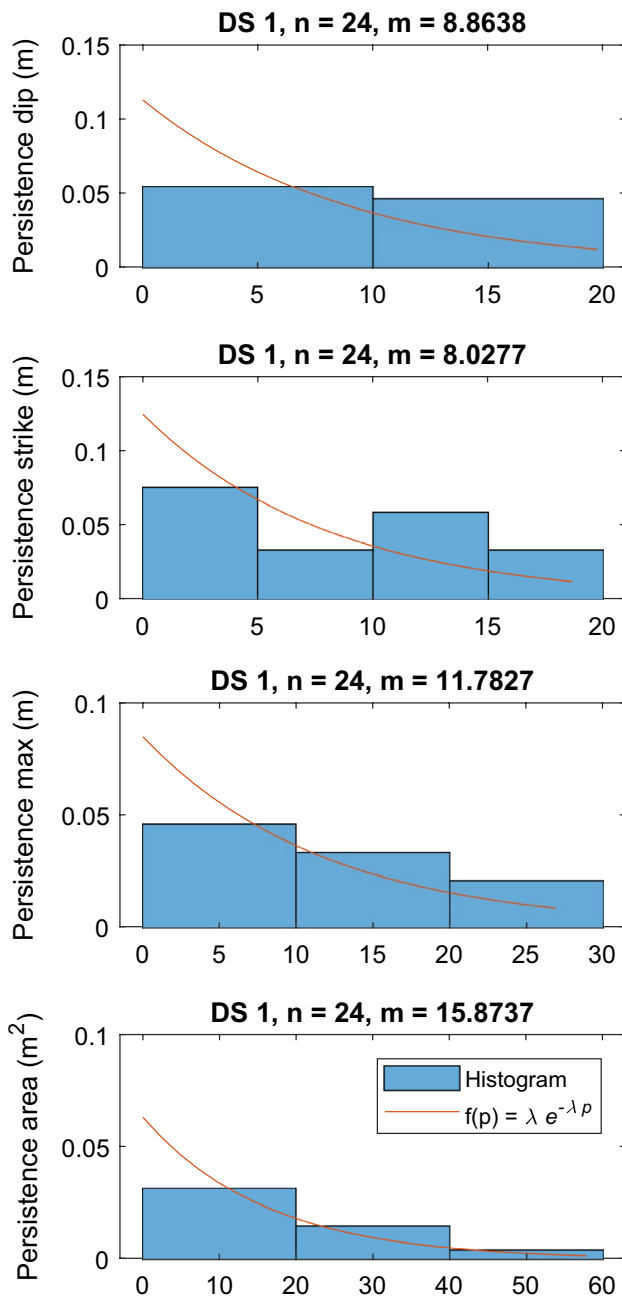


**Fig. 16** Case study 3. Measured persistence (m) in the direction of dip, strike, maximum length within the convex hull and area ( $\text{m}^2$ )

clusters were also merged, and a realistic persistence measure was provided. However, small clusters were not successfully merged because of irregularities.

Extraction of the orientation of discontinuity sets can affect the results, and therefore, an optimum application of the proposed method requires: (1) a solid background in structural geology and rock mechanics; (2) the use of supporting material such as field photographs and (3) visual

inspection and validation of the results. In addition, other difficulties were found (and discussed within the text) when addressing high persistence values of low normal spacing discontinuities, along with their waviness. Finally, it is important to emphasize that the measured persistence in case study 2 was limited by the excavation diameter and the span of the tunnel. Limitations will always be present depending on the size of the sample window used. As a result, the maximum value of persistence that can be measured will always be the size of the 3D point cloud from the study area.

## 5.2 K Threshold for Merging Clusters

Case study 1 showed that coplanar clusters could not be merged as a single discontinuity when the normal spacing is small with respect to the standard deviation ( $\sigma$ ) of the point-plane distances. Therefore, it is reasonable to consider the establishment of a test to assess the value of parameter  $k$ .

It is important to be aware of these errors because if non-coplanar clusters are merged, lower discontinuity persistence values are measured. Representative discontinuity normal spacing should be greater than the distance of merging clusters to minimize incorrect classifications, according to Eq. (4). For this purpose, the following equations are proposed:

$$s \gg k \times (\sigma_1 + \sigma_2), \quad (12)$$

$$k \times (\sigma_1 + \sigma_2) \gg s_{\text{coplanar-clusters}}. \quad (13)$$

$s$  is the normal spacing of the considered discontinuity set,  $\sigma_1$ ,  $\sigma_2$  and  $k$  are the parameters of Eq. (4) and  $s_{\text{coplanar-clusters}}$  is the representative normal spacing of coplanar clusters. The spacing of coplanar clusters is related to operator error and non-planarity of discontinuities.

In case study 1, the normal spacing ( $s$ ) of the discontinuity set 3 is 0.1 m. On the one hand, the standard deviation ( $\sigma$ ) of each cluster is approximately 0.001 m. If  $k$  is set to 3,  $k \times (\sigma_1 + \sigma_2)$  is 0.006, lower than 0.1. On the other hand, the normal spacing of coplanar clusters is approximately 0.006 m. Consequently, the value of  $k$  should be greater than 3 to merge coplanar clusters according to Eq. (13).

In case study 2, considering discontinuity set 1 and coplanar clusters 6 and 21, parameter  $D$  is  $-7.0593$  and  $-7.134$ , respectively, and standard deviation ( $\sigma$ ) is 0.0134 and 0.0498, respectively. The mean normal spacing is 0.35 m and the normal spacing between coplanar clusters is approximately 0.1 m. The test is applied according to Eqs. (12) and (13), and Eqs. (14) and (15) showing that in this case, a  $k=3$  is appropriate. However, there were difficulties to apply to the proposed method in case study 2, when discontinuities present significant waviness, as shown in Fig. 12.

$$0.35 \gg 3 \times (0.0134 + 0.0498) = 0.189, \quad (14)$$

$$3 \times (0.0134 + 0.0498) = 0.189 \gg 0.1. \quad (15)$$

Equations (12) and (13) also show when the proposed method can be applied and when not. Considering a discontinuity set, its discontinuity normal spacing ( $s$ ) and the normal spacing of coplanar clusters ( $s_{\text{coplanar-clusters}}$ ), the method can be applied if:

$$s \gg s_{\text{coplanar-clusters}}. \quad (16)$$

Case study 3 consists of a typical rock slope, in which the bedding plane is sub-vertical. Coplanar clusters 9 and 17 were selected to discuss the application of the proposed method. Their  $D$  values are  $-70.9279$  and  $-70.6047$ , and their standard deviations are  $0.0563$  and  $0.1141$  m, respectively. The normal spacing of coplanar clusters ( $s_{\text{coplanar-clusters}}$ ) is estimated as  $0.3$  m. The  $k$  parameter was set to 3. Equations (17) and (18) apply the test presented in Eqs. (12) and (13). It can be observed that, despite the inequations being fulfilled, the ratio is approximately 2. Consequently, this method can indeed be applied, but special attention is necessary.

$$1.1 \gg 3 \times (0.0563 + 0.1141) = 0.5112, \quad (17)$$

$$3 \times (0.0563 + 0.1141) = 0.5112 \gg 0.3. \quad (18)$$

### 5.3 Precision and Scanner Range Implications

The use of LiDAR-derived datasets requires consideration of the influence of: (1) accuracy (instrumental and operational) and (2) resolution and truncation.

The consideration of accuracy leads to the establishment of precision. Planar discontinuities present a standard deviation ( $\sigma$ ), which is calculated using the point-plane distances and depends on several parameters (of which one of the main is instrumental uncertainty). If a close-range TLS is considered, for instance the 3D laser scanner Leica C10, manufacturer specifications indicate angular accuracy  $12''$ , distance accuracy 4 mm and noise 2 mm at 50 m (Leica Geosystems 2011). Additionally, recent laboratory tests show that when scanning approximately at 10 m, close range error is less than 1 mm (Riquelme et al. 2017). According to the 68–95–99.7 rule of normal datasets, 99.7% of data is represented in the interval  $[-3\sigma, 3\sigma]$ . Consequently, it is reasonable to consider a precision of 0.1 mm for LiDAR-derived data.

Special considerations must be made for long-range TLS. The raw range accuracy of TLS model ILRIS 3D is 7 mm at 100 m (Teledyne Optech Incorporated 2017), and the laser beam footprint of a TLS model RIEGL VZ-6000 is 15 mm at exit and 240 mm at 2000 m (RIEGL 2017). Therefore, when using long-range instruments, the order of magnitude of the error is 10 mm. Using a precision of 0.1 mm would

not lead to errors in terms of internal operations and it can be concluded that a precision of 0.1 mm is adequate for close and long-range scanners.

Regarding resolution and truncation, the Effective Instantaneous Field of View (EIFOV) is a resolution measure for the sampling interval and the laser beamwidth (Lichti and Jamtsho 2006). According to Sturzenegger et al. (2007), this parameter defines the maximum resolution that can be obtained for a specific distance, so the longer range, the larger the footprint size. As the principal effect of resolution is data truncation, surfaces smaller than a threshold value cannot be measured. Application of the proposed methodology requires the footprint size to be sufficiently small to detect discontinuity planes and discontinuity normal spacing.

### 5.4 Sensitivity Analysis of the Proposed Methodology

Simplistic case study 1 enables a comprehensive discussion on the sensitivity of the proposed methodology. Figure 9a illustrates an interesting issue that affects the results. The top of the cubes is identified as a single cluster of points and defines a plane of a discontinuity set. The plane, depicted in red, is defined by the orientation of the principal pole extracted in Fig. 8a. The plane is adjusted using the least squared method, so the centroid of the cluster fits perfectly. However, angular deviation is observed, as points located on the top of the figure are below the plane and those placed on the lower part of the figure are above the plane. When two ‘coplanar’ clusters are separated, the angular deviation would result in both being considered as two different planes and consequently the measured persistence will be low.

The angular deviation of the plane is due to the extraction process utilized. Herein, the plane was extracted using the DSE software, and therefore, was controlled by the following processes. First, the number of points, density and error of the point clouds affect the density of the poles. The higher the noise, the more inaccurate is the non-parametric calculated function. Another source of error is related to the nature of the scanned surface: irregular, with presence of vegetation, soils or non-planar. Those points that do not belong to discontinuities will introduce poles in the stereographic analysis that will ‘contaminate’ the density function. Therefore, if the contaminated poles are close to the orientation of the discontinuity set, the local maximum of the pole density function will be displaced, and the orientation of the extracted plane will be slightly rotated. Additionally, the number of neighbours used to calculate the normal vector of each point has a significant effect on its value (Riquelme et al. 2014). The higher the number of neighbours used, the better the convergence to a mean value. However, details of the surface can be lost, and additional computing resources

are needed. Experience shows that using 30 neighbours generally provides satisfactory results.

Second, the number of bins used in the kernel density estimation (KDE) (Botev et al. 2010) can also affect the mean value. The higher the number of bins, the more precise the value extracted. However, this can also result in artefacts. Experience shows that 64 or 128 bins generally provide acceptable results.

Third, the assignment of points to a principal pole is also important. Once a principal pole is extracted, the closest poles are assigned to it. This process is controlled by the angle defined by their vectors. The higher the angle, the more irregular the surface identified as a plane. As stated in the beginning of this work, discontinuities are not planes but surfaces with roughness and waviness, so this fact must be considered. Irregular surfaces can seriously hinder the application of the proposed method. Experience shows that using a value of 30° generally provides good results.

Fourth, the clustering process is the final operation that can affect the results. The clustering process is performed through the density-based algorithm (DBSCAN) (Ester et al. 1996). It is highly recommended to use a uniform density of points to obtain optimal results. Otherwise, the clustering process will lead to poor results. Once the clustering process is completed, small clusters will be automatically created (e.g., clusters of 10 points). Although these clusters could be part of actual discontinuity planes, they could also be noise. Therefore, it is convenient to remove clusters that exhibit a size lower than a specific predefined threshold value. If these clusters are not removed, they will provide very small persistence values when identified as isolated planes or could provide extremely high persistence values if highly separated and identified as coplanar. A recommendable threshold value is 100 points per cluster, although this threshold also depends on the point spacing.

## 6 Conclusions

A new methodology was presented herein to measure discontinuity persistence using 3D point clouds. The proposed approach was designed to estimate the true persistence rather, in opposition to traditional approaches that focus on estimating the “visible persistence”. To this end, the proposed algorithm groups the different patches of discontinuity planes outcropping on the rock mass that can be geometrically classified as belonging to the same discontinuity plane. The algorithm is described herein, along with its applicability to three different case studies.

This work showed that measured persistence corresponded to the expected values. However, the use of 3D point clouds implied in the testing of several conditions prior

to the application of the proposed methodology. First, the resolution of the instrument (when 3D laser scanners are used) can affect data, especially when long-range TLS is used. Second, two tests were suggested to check the applicability of the method to the analysed data. This work also highlighted the need of considerable experience and geological knowledge in the application of the proposed automatic persistence measurement method.

Future efforts should focus on: (1) validating the presented approach with in-depth measurements of discontinuity persistence with new techniques of site investigation; and (2) investigating real persistence as a continuous function rather than a unique value.

**Acknowledgements** This work was partially funded by the University of Alicante (vigrob-157 Project, GRE14-04 Project and GRE15-19 Project), the Spanish Ministry of Economy, Industry and Competitiveness (MINECO), the State Agency of Research (AEI) and the European Funds for Regional Development (FEDER) (projects TEC2017-85244-C2-1-P and TIN2014-55413-C2-2-P) and the Spanish Ministry of Education, Culture and Sport (project PRX17/00439). A. Abellán would like to acknowledge the support received from the H2020 Program of the European Commission under the Marie Skłodowska-Curie Individual Fellowship [MSCA-IF-2015-705215].

## References

- Abellán A, Derron M-H, Jaboyedoff M (2016) ‘Use of 3D point clouds in geohazards’ special issue: current challenges and future trends. *Remote Sens* 8:130. <https://doi.org/10.3390/rs8020130>
- Alameda P (2014) Aplicación de nuevas metodologías de adquisición de datos para el análisis de estabilidad de taludes: casos de estudio en materiales foliados de la Cordillera Bética. University of Granada, Spain
- Assali P, Grussenmeyer P, Villemain T, Pollet N, Viguer F (2016) Solid images for geostructural mapping and key block modeling of rock discontinuities. *Comput Geosci* 89:21–31. <https://doi.org/10.1016/j.cageo.2016.01.002>
- Baecher GB (1983) Statistical analysis of rock mass fracturing. *J Int Assoc Math Geol* 15:329–348. <https://doi.org/10.1007/BF01036074>
- Barton N, Choubey V (1977) The shear strength of rock joints in theory and practice. *Rock Mech* 10:1–54
- Botev ZI, Grotowski JF, Kroese DP (2010) Kernel density estimation via diffusion. *Ann Stat* 38:2916–2957. <https://doi.org/10.1214/10-AOS799>
- Cano M, Tomás R (2013) Characterization of the instability mechanisms affecting slopes on carbonatic Flysch: Alicante (SE Spain), case study. *Eng Geol* 156:68–91. <https://doi.org/10.1016/j.enggeo.2013.01.009>
- Chen N, Kemeny J, Jiang Q, Pan Z (2017) Automatic extraction of blocks from 3D point clouds of fractured rock. *Comput Geosci* 109:149–161. <https://doi.org/10.1016/J.CAGEO.2017.08.013>
- Dershowitz WS (1985) Rock joint systems. Ph. D. Thesis, Massachusetts Institute of Technology
- Dershowitz WS, Einstein HH (1988) Characterizing rock joint geometry with joint system models. *Rock Mech Rock Eng* 21:21–51. <https://doi.org/10.1007/BF01019674>
- Einstein HH, Veneziano D, Baecher GB, O'Reilly KJ (1983) The effect of discontinuity persistence on rock slope stability. *Int J*

- Rock Mech Min Sci Geomech Abstr 20:227–236. [https://doi.org/10.1016/0148-9062\(83\)90003-7](https://doi.org/10.1016/0148-9062(83)90003-7)
- Ester M, Kriegel H, Sander J, Xu X (1996) A density-based algorithm for discovering clusters in large spatial databases with noise. In: Simoudis E, Han J, Fayyad U (eds) Second international conference on knowledge discovery and data mining. AAAI Press, Portland, Oregon, pp 226–231
- García-Sellés D, Falivene O, Arbués P, Gratacos O, Tavani S, Muñoz JA (2011) Supervised identification and reconstruction of near-planar geological surfaces from terrestrial laser scanning. Comput Geosci 37:1584–1594. <https://doi.org/10.1016/j.cageo.2011.03.007>
- Gigli G, Casagli N (2011) Semi-automatic extraction of rock mass structural data from high resolution LIDAR point clouds. Int J Rock Mech Min Sci 48:187–198. <https://doi.org/10.1016/j.ijrmms.2010.11.009>
- Goodman RE (1989) Introduction to rock mechanics, 2nd edn. Wiley, New York
- Haneberg W (2007) Directional roughness profiles from three-dimensional photogrammetric or laser scanner point clouds. In: Eberhardt E, Stead D, Morrison T (eds) Rock mechanics: meeting society's challenges and demands. Taylor & Francis, Vancouver, pp 101–106
- Haneberg WC (2008) Using close range terrestrial digital photogrammetry for 3-D rock slope modeling and discontinuity mapping in the United States. Bull Eng Geol Environ 67:457–469. <https://doi.org/10.1007/s10064-008-0157-y>
- Hudson JA, Priest SD (1983) Discontinuity frequency in rock masses. Int J Rock Mech Min Sci 20:73–89. [https://doi.org/10.1016/0148-9062\(83\)90329-7](https://doi.org/10.1016/0148-9062(83)90329-7)
- Humair F, Abellán A, Carrea D, Matasci B, Epard J-L, Jaboyedoff M (2015) Geological layers detection and characterisation using high resolution 3D point clouds: example of a box-fold in the Swiss Jura Mountains. Eur J Remote Sens 48:541–568. <https://doi.org/10.5721/EuJRS20154831>
- International Society for Rock Mechanics (1978) International society for rock mechanics commission on standardization of laboratory and field tests: Suggested methods for the quantitative description of discontinuities in rock masses. Int J Rock Mech Min Sci Geomech Abstr 15:319–368. [https://doi.org/10.1016/0148-9062\(79\)91476-1](https://doi.org/10.1016/0148-9062(79)91476-1)
- Jaboyedoff M, Metzger R, Oppikofer T, Couture R, Derron M-H, Locat J, Turmel D (2007) New insight techniques to analyze rock-slope relief using DEM and 3D-imaging cloud points: COLTOP-3D software. In: Francis T (ed) Rock mechanics: Meeting Society's challenges and demands. Proceedings of the 1st Canada—U.S. Rock Mechanics Symposium, Vancouver, Canada, May 27–31, 2007. pp 61–68
- Jaboyedoff M, Oppikofer T, Abellán A, Derron M-, Loyer HM-H, Metzger A, Pedrazzini R A (2012) Use of LIDAR in landslide investigations: a review. Nat hazards 61:5–28. <https://doi.org/10.1007/s11069-010-9634-2>
- Jordá Bordehore L, Riquelme A, Cano M, Tomás R (2017) Comparing manual and remote sensing field discontinuity collection used in kinematic stability assessment of failed rock slopes. Int J Rock Mech Min Sci 97:24–32. <https://doi.org/10.1016/j.ijrmms.2017.06.004>
- Khoshelham K, Altundag D, Ngan-Tillard D, Menenti M (2011) Influence of range measurement noise on roughness characterization of rock surfaces using terrestrial laser scanning. Int J Rock Mech Min Sci 48:1215–1223. <https://doi.org/10.1016/j.ijrmms.2011.09.007>
- Kurz TH, Buckley SJ, Howell JA, Schneider D (2011) Integration of panoramic hyperspectral imaging with terrestrial lidar data. Photogramm Rec 26:212–228. <https://doi.org/10.1111/j.1477-9730.2011.00632.x>
- Lai P, Samson C, Bose P (2014) Surface roughness of rock faces through the curvature of triangulated meshes. Comput Geosci 70:229–237. <https://doi.org/10.1016/j.cageo.2014.05.010>
- Lato MJ, Bevan G, Fergusson M (2012) Gigapixel imaging and photogrammetry: development of a new long range remote imaging technique. Remote Sens 4:3006–3021. <https://doi.org/10.3390/rs4103006>
- Lato MJ, Kemeny J, Harrap RM, Bevan G (2013) Rock bench: Establishing a common repository and standards for assessing rockmass characteristics using LiDAR and photogrammetry. Comput Geosci 50:106–114. <https://doi.org/10.1016/j.cageo.2012.06.014>
- Leica (2016) Cyclone v9.1
- Leica Geosystems AG (2011) Leica ScanStation C10 data sheet. Heerbrugg, Switzerland
- Lichti DD, Jamtsho S (2006) Angular resolution of terrestrial laser scanners. Photogramm Rec 21:141–160. <https://doi.org/10.1111/j.1477-9730.2006.00367.x>
- Longoni L, Arosio D, Scaioni M, Papini M, Zanzi L, Roncella R, Brambilla D (2012) Surface and subsurface non-invasive investigations to improve the characterization of a fractured rock mass. J Geophys Eng 9:461–472. <https://doi.org/10.1088/1742-2132/9/5/461>
- Mauldon M (1994) Intersection probabilities of impersistent joints. Int J Rock Mech Min Sci 31:107–115. [https://doi.org/10.1016/0148-9062\(94\)92800-2](https://doi.org/10.1016/0148-9062(94)92800-2)
- Micheletti N, Chandler JH, Lane SN (2015) Investigating the geomorphological potential of freely available and accessible structure-from-motion photogrammetry using a smartphone. Earth Surf Process Landforms 40:473–486. <https://doi.org/10.1002/esp.3648>
- Oppikofer T, Jaboyedoff M, Blikra L, Derron M-, Metzger H R (2009) Characterization and monitoring of the Åknes rockslide using terrestrial laser scanning. Nat Hazards Earth Syst Sci 9:1003–1019. <https://doi.org/10.5194/nhess-9-1003-2009>
- Oppikofer T, Jaboyedoff M, Pedrazzini A, Derron M-, Blikra H L (2011) Detailed DEM analysis of a rockslide scar to characterize the basal sliding surface of active rockslides. J Geophys Res Earth Surf. <https://doi.org/10.1029/2010JF001807>
- Ortega OJ, Marrett RA, Laubach SE (2006) A scale-independent approach to fracture intensity and average spacing measurement. Am Assoc Pet Geol Bull 90:193–208. <https://doi.org/10.1306/08250505059>
- Park HJ, West TR, Woo I (2005) Probabilistic analysis of rock slope stability and random properties of discontinuity parameters, Interstate Highway 40, Western North Carolina, USA. Eng Geol 79:230–250. <https://doi.org/10.1016/j.enggeo.2005.02.001>
- Priest SD, Hudson JA (1981) Estimation of discontinuity spacing and trace length using scanline surveys. Int J Rock Mech Min Sci 18:183–197. [https://doi.org/10.1016/0148-9062\(81\)90973-6](https://doi.org/10.1016/0148-9062(81)90973-6)
- Rahman Z, Slob S, Hack HRGK (2006) Deriving roughness characteristics of rock mass discontinuities from terrestrial laser scan data. In: Proceedings of 10th IAEG congress: engineering geology for tomorrow's cities, Nottingham, United Kingdom. pp 1–12
- RIEGL (2017) RIEGL VZ-6000 3D very long range terrestrial laser scanner with online waveform processing terrestrial laser scanning
- Riquelme AJ, Abellán A, Tomás R, Jaboyedoff M (2014) A new approach for semi-automatic rock mass joints recognition from 3D point clouds. Comput Geosci 68:38–52. <https://doi.org/10.1016/j.cageo.2014.03.014>
- Riquelme A, Abellán A, Tomás R (2015) Discontinuity spacing analysis in rock masses using 3D point clouds. Eng Geol 195:185–195. <https://doi.org/10.1016/j.enggeo.2015.06.009>
- Riquelme A, Tomás R, Cano M, Abellán A, Tomás R, Abellán A (2016) Using open-source software for extracting geomechanical parameters of a rock mass from 3D point clouds: discontinuity Set Extractor and SMRTool. In: Ulusay R, Aydan Ö, Gercek H, Hindistan M, Tuncay E (eds) Rock mechanics & rock engineering:

- from the past to the future. CRC Press, Taylor & Francis Group, London, pp 1091–1096
- Riquelme A, Ferrer B, Mas D (2017) Use of high-quality and common commercial mirrors for scanning close-range surfaces using 3D laser scanners: a laboratory experiment. *Remote Sens* 9:1152. <https://doi.org/10.3390/rs9111152>
- Ruiz-Carulla R, Corominas J, Mavrouli O (2017) A fractal fragmentation model for rockfalls. *Landslides* 14:875–889. <https://doi.org/10.1007/s10346-016-0773-8>
- Shang J, Hencher SR, West LJ, Handley K (2017) Forensic excavation of rock masses: a technique to investigate discontinuity persistence. *Rock Mech Rock Eng* 50:2911–2928. <https://doi.org/10.1007/s00603-017-1290-3>
- Slob S, Turner AK, Bruining J, Hack HRGK (2010) Automated rock mass characterisation using 3-D terrestrial laser scanning. TU Delft, Delft University of Technology, Delft
- Sturzenegger M, Stead D (2009a) Close-range terrestrial digital photogrammetry and terrestrial laser scanning for discontinuity characterization on rock cuts. *Eng Geol* 106:163–182. <https://doi.org/10.1016/j.enggeo.2009.03.004>
- Sturzenegger M, Stead D (2009b) Quantifying discontinuity orientation and persistence on high mountain rock slopes and large landslides using terrestrial remote sensing techniques. *Nat Hazards Earth Syst Sci* 9:267–287
- Sturzenegger M, Yan M, Stead D, Elmo D (2007) Application And Limitations of Ground-based Laser Scanning In Rock Slope Characterization. In: Eberhardt E, Stead D, Morrison T (eds) 1st Canada—U.S. Rock Mechanics Symposium. American Rock Mechanics Association, Vancouver, Canada, pp 29–36
- Sturzenegger M, Stead D, Elmo D (2011) Terrestrial remote sensing-based estimation of mean trace length, trace intensity and block size/shape. *Eng Geol* 119:96–111. <https://doi.org/10.1016/j.enggeo.2011.02.005>
- Tatone BSA, Grasselli G (2010) A new 2D discontinuity roughness parameter and its correlation with JRC. *Int J Rock Mech Min Sci* 47:1391–1400. <https://doi.org/10.1016/j.ijrmms.2010.06.006>
- Teledyne Optech Incorporated (2017) ILRIS-LR terrestrial laser scanner. Canada
- Tuckey Z, Stead D (2016) Improvements to field and remote sensing methods for mapping discontinuity persistence and intact rock bridges in rock slopes. *Eng Geol* 208:136–153. <https://doi.org/10.1016/j.enggeo.2016.05.001>
- Ullman S (1979) The interpretation of visual motion. Massachusetts Inst of Technology Pr, Cambridge
- Vaskou P (2016) Structural characterization of faults and fractures in underground works. In: Ulusay R, Aydan O, Gercek H, Hindistan MA, Tuncay E (eds) Rock mechanics and rock engineering: from the past to the future. CRC Press, Boca Raton, pp 99–104
- Vivas J, Hunt C, Stead D, Allen DM, Elmo D (2015) Characterising groundwater in rock slopes using a combined remote sensing—numerical modelling approach. In: 13th ISRM Int. Congr. Rock Mech
- Vöge M, Lato MJ, Diederichs MS (2013) Automated rockmass discontinuity mapping from 3-dimensional surface data. *Eng Geol* 164:155–162. <https://doi.org/10.1016/j.enggeo.2013.07.008>
- Wang X, Zou L, Shen X, Ren Y, Qin Y (2017) A region-growing approach for automatic outcrop fracture extraction from a three-dimensional point cloud. *Comput Geosci* 99:100–106. <https://doi.org/10.1016/j.cageo.2016.11.002>
- Zhang L (2006) Rock discontinuities. In: Zhang L (eds) Engineering properties of rocks, 4th edn. Elsevier, Amsterdam, pp 226–230
- Zhang L, Einstein HH (2000) Estimating the intensity of rock discontinuities. *Int J Rock Mech Min Sci* 37:819–837. [https://doi.org/10.1016/S1365-1609\(00\)00022-8](https://doi.org/10.1016/S1365-1609(00)00022-8)

**Publisher's Note** Springer Nature remains neutral with regard to jurisdictional claims in published maps and institutional affiliations.